THE JOURNAL OF PHYSICAL CHEMISTRY A

Article

pubs.acs.org/JPCA

NMR Studies of Solid Pentachlorophenol-4-Methylpyridine Complexes Exhibiting Strong OHN Hydrogen Bonds: Geometric H/D Isotope Effects and Hydrogen Bond Coupling Cause Isotopic Polymorphism

Brenda C. K. Ip,[†] Ilya G. Shenderovich,[†,‡,∥] Peter M. Tolstoy,[†,‡,⊥] Jaroslaw Frydel,[†] Gleb S. Denisov,[‡] Gerd Buntkowsky,[§] and Hans-Heinrich Limbach*[,†]

[†]Institut für Chemie und Biochemie, Freie Universität Berlin, Takustrasse 3, D-14195 Berlin, Germany

[‡]St. Petersburg State University, 198504 St. Petersburg, Russian Federation

[§]Eduard-Zintl-Institut für Anorganische und Physikalische Chemie, Technische Universität Darmstadt, Petersenstr. 20, D-64287 Darmstadt, Germany

Supporting Information

ABSTRACT: We have studied the hydrogen bond interactions of ^{15}N labeled 4-methylpyridine (4-MP) with pentachlorophenol (PCP) in the solid state and in polar solution using various NMR techniques. Previous spectroscopic, X-ray, and neutron crystallographic studies showed that the triclinic 1:1 complex (4-MPPCP) exhibits the strongest known intermolecular OHN hydrogen bond in the solid state. By contrast, deuteration of the hydrogen bond gives rise to the formation of a monoclinic structure exhibiting a weaker hydrogen bond. By performing NMR experiments at different deuterium fractions and taking advantage of dipolar $^{1}H-^{15}N$ recoupling under combined fast MAS and ^{1}H decoupling, we provide an explanation of the origin of the isotopic polymorphism of 4-MPPCP and improve previous chemical shift correlations for OHN hydrogen bonds. Because of anharmonic ground state vibrations, an ODN hydrogen bond in the triclinic form exhibits a shorter oxygen−hydron and a longer oxygen−nitrogen distance as compared to surrounding OHN hydrogen bonds, which also implies a reduction of the local dipole moment. The dipole−dipole interaction between adjacent coupled OHN hydrogen bonds which determines the structure of triclinic 4-MPPCP is then reduced by deuteration, and other interactions become dominant, leading to the monoclinic form. Finally, the observation of stronger OHN hydrogen bonds by ^{1}H NMR in polar solution as compared to the solid state is discussed.

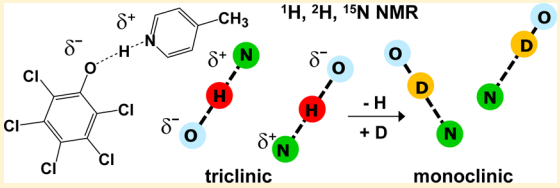

INTRODUCTION

The quantum nature of hydrogen plays an important role in hydrogen transfer processes and hydrogen bonding. Therefore, in order to understand both phenomena, a close interaction between experiment and theory is required.[1] Hydrogen bond mediated acid−base interactions of amino acid side chains and cofactors in proteins are especially challenging, as they represent key features for their function.[2,3] Unfortunately, it is difficult to localize protons using X-ray diffraction techniques and hence to elucidate local electrostatics essential for the biomolecular functions. Neutron diffraction has been applied only very recently to larger proteins, where a high resolution necessary for the localization of proton positions is still difficult to obtain.[4−6] Therefore, various NMR methods have been used to localize protons in hydrogen bonds, in particular the elucidation of dipolar $^{1}H-^{1}H$ couplings,[7−9] $^{1}H-^{15}N$ couplings,[7,10−13] and $^{1}H-^{13}C$ couplings[14] in suitably isotopically labeled systems. In large molecules, the determination of dipolar couplings by NMR is difficult. Therefore, the determination of NMR chemical shifts and of their relation to molecular geometries using quantum-mechanical calculations has become an important tool of "NMR crystallography".[15] Particularly useful is the determination of H/D isotope effects on hydrogen bond geometries in the solid state caused by anharmonic ground state vibrations. The resulting H/D isotope effects on the corresponding NMR chemical shifts are more sensitive to hydrogen bond structures as compared to the chemical shifts themselves.[16]

Recently,[17] some of us have demonstrated that the position of a functional proton between an aspartic acid residue and the pyridine ring of vitamin B6 in a large enzyme can be estimated from ^{15}N NMR chemical shifts. The latter have been shown to correlate with hydrogen bond geometries established by neutron diffraction or NMR spectroscopy of suitable model systems.[18−22] Thus, changes of the geometries of OHN-hydrogen bonds in protein active sites between the crystalline state and aqueous solution can be followed by ^{15}N NMR. Such

Special Issue: A: Jorn Manz Festschrift

Received: June 14, 2012
Revised: July 28, 2012
Published: August 3, 2012

a comparison is important to establish structure−function relationships.

However, in the $^{1}H-^{15}N$ chemical shift correlations proposed,[20b] solid state data for the strongest OHN hydrogen bonds were scarce. In order to fill this gap, we undertook the present NMR study of the 1:1 complex of 4-methylpyridine with pentachlorophenol (4-MPPCP, Figure 1). Majerz et al.

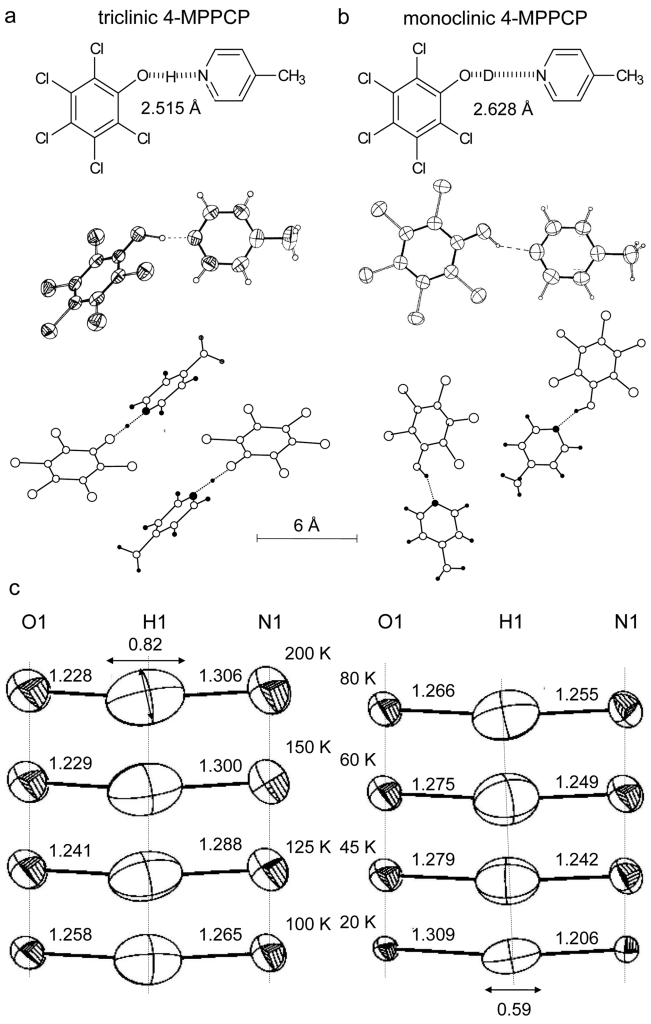

Figure 1. (a) X-ray structure of 4-MPPCP-*h* and (b) of 4-MPPCP-*d* according to Malarski et al.[26,29] (files RAKQOJ and GADGUN01 of the Cambridge Structural Database CSD). (c) Neutron diffraction crystal structure of 4-MPPCP according to Steiner et al.[28] Displacement ellipsoids are drawn at the 50% probability level. The equidistant H atom position occurs at around 90 K. The numbers refer to distances in Å.

have shown using ^{35}Cl NQR,[23,24] IR, UV/vis,[25] and X-ray crystallography[26] that this complex adopts a triclinic crystal structure where it exhibits the shortest known intermolecular O···N distance of about 2.5 Å, as illustrated in Figure 1a. The asymmetric unit contains a single complex, but the packing diagram indicates that two 1:1 complexes form a pair with antiparallel hydrogen bonds. Lowering the temperature down to 80 K indicated a shortening of the O−H···N but not of the O−D···N hydrogen bond.[27] These findings were confirmed by neutron diffraction studies by Steiner et al.[28] which revealed the presence of a quasi-symmetric hydrogen bond. Lowering the temperature not only shortened the O···N bond length but also shifted the proton slightly across the hydrogen bond center, as illustrated in Figure 1c. At the same time, the volume of the thermal displacement ellipsoids of the proton decreased.

In addition to these exceptional properties, Majerz et al. found that 4-MPPCP adopts a monoclinic crystal structure when the hydrogen bond is deuterated, as illustrated in Figure 1b.[29] The O−D···N bond weakens substantially as the O···N distance is increased to 2.628 Å and as the deuteron is displaced toward oxygen. The packing diagram indicates a perpendicular arrangement of two adjacent complexes. Crystal structure changes of hydrogen bonded systems upon deuteration of mobile proton sites have been observed before.[30] Related cases where replacement of OHN by ODN hydrogen bonds leads to a different crystal structure are the cases of crystalline 1:1 isonicotinamide-oxalic acid complexes[31] 3,5-pyridine-dicarboxylic acid[32] and of glycine.[33] Recently, crystal structure changes after substituting all H atoms of organic crystals by D have been observed, for example, in the cases of pyridine,[34] pyridine-*N*-oxide,[35] or L-alanine.[36] Harbison et al.[37] have proposed the term "isotopomeric polymorphism" to describe a crystal structure change induced by isotopic substitution. Here, we use the term "isotopic polymorphism" proposed by Boese et al.[34] which is in better agreement with IUPAC rules.[38]

Harbison et al.[37] have pioneered ^{1}H and ^{2}H solid state MAS NMR in order to characterize the isotopic polymorphism of 4-MPPCP in more detail. They found a low-field ^{1}H signal around 18 ppm for the strong hydrogen bond in the triclinic modification of 4-MPPCP. This value increased to about 20 ppm when the temperature was lowered.[39] It was also found that triclinic 4-MPPCP could be deuterated up to almost 50%; at higher deuterium fractions, the solids consisted of mixtures of the two polymorphs. ^{2}H MAS NMR measurements of partially deuterated triclinic 4-MPPCP indicated a decrease of the ^{2}H quadrupole coupling constant when the temperature was lowered, in agreement with a strengthening of the hydrogen bond. By contrast, ^{1}H NMR high field shifts to about 12−14 ppm were observed for monoclinic 4-MPPCP at higher deuterium fractions.

In order to elucidate the origin of the isotopic polymorphism of 4-MPPCP, Harbison et al.[39] have measured the hydrogenic vibrations of triclinic 4-MPPCP using inelastic neutron scattering (INS). They showed that the zero point energy difference between the OHN and ODN bonds vanishes in the case of the triclinic form but is about 500 cm^{-1} in the case of the monoclinic form. This finding can explain the preference of D for the monoclinic form, as generally D enriches in sites with weaker hydrogen bonds associated with larger zero-point energies. Some of us have observed similar equilibrium isotope effects, i.e., isotopic fractionation in the case of pyridine-acid complexes in solution.[18g] A remaining puzzle with the explanation of the isotopic polymorphism in terms of zero-point energy changes was why the monoclinic form is not observed at deuterium fractions lower than 0.5. That observation is difficult to explain in terms of a single hydrogen bond approach and might require consideration of the interaction between different complexes in order to understand the isotopic polymorphism.

In order to fill the NMR-geometry correlation gap of strong OHN hydrogen bonds and in order to improve our knowledge of geometric hydrogen bond isotope effects and isotopic polymorphism, we have synthesized ^{15}N labeled 4-MPPCP and have performed high-resolution ^{15}N solid state NMR studies on this compound in addition to ^{1}H and ^{2}H NMR experiments.

dx.doi.org/10.1021/jp305863n | J. Phys. Chem. A 2012, 116, 11370−11387

On one hand, the new data improve the $^{1}H-^{15}N$ chemical shift correlation established previously[20b] for OHN hydrogen bonds to pyridine and its derivatives. Using these correlations, the geometric H/D isotope effects could be established for various forms of 4-MPPCP. On the other hand, the analysis of these effects directly leads to an improved understanding of the isotopic polymorphism of 4-MPPCP and possibly also of other systems.

This paper is organized as follows. In the next section, we describe the synthesis of ^{15}N labeled 4-MP and the preparation of various samples of its complexes with PCP. We also describe shortly the analysis used to correlate NMR parameters with hydrogen bond geometries. Then, we report the results of our ^{1}H, ^{2}H, and ^{15}N solid state NMR experiments. For comparison, we have performed additional low-temperature ^{1}H and ^{15}N NMR experiments on this complex in the polar freonic liquid CDF_3/CDF_2Cl in order to study the influence of the medium polarity on 4-MPPCP. Then, our results are discussed in two parts. The first part is devoted to NMR-hydrogen bond correlations and H/D isotope effects on 4-MPPCP in comparison with related complexes, and the second part, to the isotopic polymorphism as well as solid-solution state and temperature effects on hydrogen bonded properties of pyridine-acid complexes.

MATERIALS AND METHODS

Synthesis of ^{15}N Labeled 4-MPPCP. The synthesis of ^{15}N-labeled 4-methylpyridine **1** was done according to Scheme 1. In a first step, the starting material ethoxy-4-methyl-3,4-dihydro-2*H*-pyran **2** was prepared according to the procedure of Longley and Emerson.[40] In the next step, **2** was let to react with $^{15}NH_4Cl$ to form 4-methylpyridine **1**, similar to the method which has been described for the ^{15}N-labeled unsubstituted pyridine by Whaley and Ott.[41] The melting point of both the protonated triclinic and the monoclinic deuterated polymorphs of 4-MPPCP was found to be 70 °C.[37] Finally, 4-MPPCP was synthesized as described below in analogy to the nonlabeled compound[29] from **1** and pentachlorophenol (Sigma-Aldrich). All synthetic procedures are included in the Supporting Information.

Scheme 1. Synthesis of 4-Methylpyridine-^{15}N According to the Procedure for the Parent Compound Pyridine-^{15}N Described Previously[41]

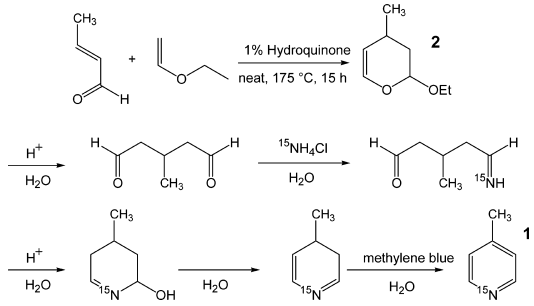

NMR Samples. Different procedures were used to prepare various samples of 4-MPPCP, which are characterized in Table 1 together with their NMR parameters obtained below.

Preparation of Triclinic 4-MPPCP via Procedure A. Triclinic nondeuterated 4-MPPCP-d_0 (sample **a**) was obtained by dissolving equivalent molar amounts of 4-methylpyridine and pentachlorophenol (Aldrich) in acetonitrile at 40 °C and by crystallization at room temperature. The product was then filtered and air-dried. Removal of solvent *in vacuo* leads to a partial removal of methylpyridine and other than 1:1 complexes are formed as shown later.

Preparation of Partially Deuterated and Deuterated Samples via Procedure B. Partially deuterated 4-MPPCP-d_x samples **b**–**d** exhibiting a deuterium fraction of x_D = 0.05, 0.45, and 0.7 in the mobile proton site were prepared as described previously.[29] 4-MPPCP-d_0 was dissolved in methanol containing the desired deuterium fraction, obtained by mixing appropriate volumes of CH_3OH and CH_3OD. For the preparation of the fully deuterated sample **e** (4-MPPCP-$d_{0.95}$)—containing a deuterium fraction of at least 0.95—pure CH_3OD was employed. In the next step, solvent was partially removed by evaporation. Finally, the concentrated solution was stored in a desiccator over a molecular sieve (4 Å), leading to crystallization.

*Preparation of Samples **f**–**h** via Procedure C.* These samples were prepared from solutions of 4-MP in CH_3OH (samples **f** and **h**) and in CH_3OD (sample **g**) in the presence of additional PCP via removal of the solvent *in vacuo*. These samples contained unequal mole fractions of 4-MP and PCP, i.e., generally $x_{4\text{-MP}}/x_{PCP} < 1$. Their relative amounts were estimated via ^{15}N solid state NMR. It turned out that the removal of the solvent *in vacuo* can also lead to a loss of 4-MP.

*Preparation of Samples **i** and **a1**.* Neat PCP (sample ***i***) was measured as purchased without further purification. Sample **a1** for liquid state NMR measurements was obtained by dissolving sample **a** in a CDF_3/CDF_2Cl mixture prepared as described previously.[18a]

Deuterium Fractions of Solid Samples. The relative deuterium contents of the different samples were checked by measuring the 90° pulse ^{2}H MAS NMR spectra under the same conditions, and by comparing the total integrated signal intensities. This procedure resulted in slight adjustments of the deuterium fractions.

NMR Spectroscopy. If not otherwise stated, high-resolution ^{1}H MAS, ^{2}H MAS, and ^{15}N MAS NMR solid state measurements were performed using a Varian Infinity Plus 600 spectrometer operating at 14 T, i.e., at a frequency of 599.97 MHz for ^{1}H, 92.10 MHz for ^{2}H, and 60.8 MHz for ^{15}N. The spectrometer was equipped with a 2.5 mm Chemagnetics-Varian variable temperature pencil probe. Low-temperature MAS operation was achieved as described previously.[42] The experimental conditions of all spectra published here are included in Table S3 of the Supporting Information. All high-resolution ^{1}H and ^{2}H MAS NMR spectra and many ^{15}N MAS NMR spectra were obtained using 90° pulses and spinning speeds of either 16 or 18 kHz. Thus, neither cross-polarization (CP) nor ^{1}H decoupling were employed in the case of the ^{15}N experiments. Some ^{15}N NMR spectra were acquired using ^{1}H decoupling (4 mm pencil probe, 12 kHz spinning speed). As high spinning speeds cause sample heating,[43] temperature settings were calibrated using the ^{15}N chemical shift thermometer TTAA described previously[44] (see the Supporting Information). Some ^{15}N CPMAS measurements were carried out on a Varian 7 T instrument operating at 30.43 MHz for ^{15}N, equipped with a 6 mm Chemagnetics-Varian variable temperature pencil probe. The spinning speeds were 6 kHz, using contact times of 5 ms.

The solid state ^{1}H and ^{2}H chemical shifts were measured using solid hexamethylbenzene (HMB, $C_{12}H_{18}$ and $C_{12}D_{18}$) as external references. With respect to solid 3-(trimethylsilyl)-

dx.doi.org/10.1021/jp305863n | J. Phys. Chem. A 2012, 116, 11370–11387

Table 1. NMR Parameters of Solid Complexes of 4-MP with PCP[a]

sample	x_D	procedure	species	T (K)	δ(OHN)	δ(ODN)	δ(OHN)	δ(ODN)	x(OHN)	x(ODN)
a	0	A	t	323	18.0					
				297	18.2		215			
				277	18.5		214			
				253	18.7		212			
				228	18.9		210			
b	0.05	B	t	297	18.2	17.5	215			
				277	18.4	17.7				
				253	18.6	18.0				
				228	18.8	18.4				
c	0.45	B	t	297	18.2	17.5	215.4	218.1	0.55	0.45
				277	18.4	17.7	212.6	214.5	0.55	0.45
				253	18.6	17.9	211.8	213.9	0.55	0.45
				228	18.8	18.2	210.7	212.4	0.55	0.45
d	0.7	B	t	297	18.2		214.9	217.4	0.21	0.04
			m_1		14.2	13.6		246.4		0.24
			m_2				244.1	244.5	0.08	0.42
			t	277	18.4		212.9	215.0	0.21	0.04
			m_1		14.2	13.6		246.2		0.24
			m_2				243.9	244.3	0.08	0.42
			t	253	18.6		210.8	212.8	0.21	0.04
			m_1		14.3	13.6		246.1		0.24
			m_2				243.8	244.2	0.08	0.42
			t	228	18.7		209.4	208.3	0.21	0.04
			m_1		14.4	13.8		245.2		0.24
			m_2				243.3	243.7	0.08	0.42
e	>0.95	B	m_1	297		13.6		246.1		
				277		13.6		246		
				253		13.6		245.4		
				228		13.7		245.2		
f	0	C	t	297	18.4		215			
			1:2[b]		12.3		166			
g	>0.95	C	m	297	13.6	13.6		245		
			1:2[b]		12.3		166			
h	0	C	1:10[c]	297	12.3		166			
i	0		PCP[d]	297	7					

[a] x_D is the global deuterium fraction. Chemical shifts δ in ppm. The margins of error of δ(OHN) and of δ(ODN) are about ±0.2 ppm, those of δ(OHN) and δ(ODN) are about ±0.5 ppm, and those of x(OHN) and x(ODN) are about ±0.05. t triclinic crystal structure, m monoclinic crystal structure. The mole fractions of the ODN hydrogen bonds were calculated from the corresponding ^{15}N line intensities of the one-pulse spectra, x(ODN) = I(ODN)/(I(OHN) + I(ODN)). [b] Solid containing 4-MP and PCP in the ratio 1:2. [c] 1:10. [d] Pure PCP.

propionic acid sodium salt (TSP, $Si(CH_3)_3-CD_2-CD_2-COO^-Na^+$), HMB exhibits an isotropic chemical shift of +1.8 ppm in the solid state and of +2.3 ppm in the liquid state (see the Supporting Information). We attribute the difference to high field shifts arising from intermolecular interactions, in agreement with the molecular packing.[45] All ^{15}N solid state chemical shifts were referenced to external solid $^{15}NH_4Cl$. The ^{15}N MAS and CPMAS spectra were processed using a line broadening of 50 Hz. No line broadening was used in the case of the ^{1}H MAS NMR spectra, and 20 Hz in the case of the ^{2}H MAS NMR spectra.

The low temperature liquid state NMR spectra using CDF_3/CDF_2Cl as solvent were recorded on a Bruker AMX-500 instrument equipped with a special probe allowing measurements down to 90 K. The ^{1}H chemical shifts were referenced to TMS, and the ^{15}N chemical shifts, internally to those of the corresponding free pyridine bases in freon. In a later stage of this study, for a comparison of the solid and liquid state ^{15}N chemical shifts, we proceeded as follows. First, we measured the solid state ^{15}N chemical shifts of the neat frozen bases with respect to solid $^{15}NH_4Cl$. They were then used individually as references for the corresponding acid–base complexes. The ^{15}N chemical shifts obtained for freon solutions were converted into the solid $^{15}NH_4Cl$ scale using the help of an external nitromethane standard.[46]

Hydrogen Bond Correlation Analysis. From the standpoint of neutron crystallography, one can associate to any hydrogen bonded system A–H···B the distances $r_1 = r_{AH}$, $r_2 = r_{HB}$, and $r_3 = r_{AB}$. This characterization is, however, not complete, as it does not take into account the shape of the proton, i.e., the volume of the thermal displacement ellipsoids arising from zero-point vibrations and from the excitation of hydrogen bond vibrations, as was illustrated in Figure 1c. It is convenient to define additionally the natural hydrogen bond coordinates q_1 and q_2 according to

$$q_1 = 0.5(r_1 - r_2), \quad q_2 = r_1 + r_2 \tag{1}$$

In the case of a linear hydrogen bond, q_1 corresponds directly to the distance of the proton with respect to the hydrogen bond center and q_2 is equal to the heavy atom distance r_{AB}.

dx.doi.org/10.1021/jp305863n | J. Phys. Chem. A 2012, 116, 11370–11387

According to the valence bond order concepts proposed by Pauling[47] and Brown,[48] one can associate to both hydrogen bond distances valence bond orders given by

$$p_1 = \exp\{-(r_1 - r_1^\circ)/b_1\} \quad \text{and}$$
$$p_2 = \exp\{-(r_2 - r_2^\circ)/b_2\} \tag{2}$$

where r_1° and r_2° represent the equilibrium distances in the fictive free diatomic units AH and HB and b_1 and b_2 describe bond order decays with increasing bond distances. Assuming that the total valency of hydrogen is unity, it follows that

$$p_1 + p_2 = \exp\{-(r_1 - r_1^\circ)/b_1\} + \exp\{-(r_2 - r_2^\circ)/b_2\} = 1 \tag{3}$$

Thus, both distances r_1 and r_2 depend on each other. Using eq 3, it is possible to express r_1 as a function of r_2 or q_1 as a function of q_2.

Gilli et al.[49] and Steiner et al.[22,50] showed the validity of this approach on the basis of a number of neutron diffraction structures contained in the Cambridge Structural Database. A more detailed analysis showed that eq 3 can describe equilibrium geometries resulting from *ab initio* calculations, i.e., cases of almost harmonic potentials for the proton motions. However, eq 3 failed for strong hydrogen bonds involving anharmonic proton potentials. Thus, eq 3 is valid only in the absence of quantum zero point vibrational effects (QZPVE) present in strong hydrogen bonds.[51]

Some of us have, therefore, proposed to calculate the corrected bond orders p_{AL} and p_{LB} of ALB hydrogen bonds as a function of the equilibrium bond orders accessible by *ab initio* calculations in the following way[20]

$$p_{AL} = \exp\{-(r_{AL} - r_1^\circ)/b_1\} = p_1 - c^L(p_1p_2)^f(p_1 - p_2) - d^L(p_1p_2)^g$$
$$p_{LB} = \exp\{-(r_{LB} - r_2^\circ)/b_2\} = p_2 + c^L(p_1p_2)^f(p_1 - p_2) - d^L(p_1p_2)^g \tag{4}$$

The parameters c^L and d^L determine the size of the isotope sensitive correction term for QZPVE. c^L describes isotope shifts along the correlation line, keeping the total bond valencies of H and of D equal to unity (eq 3). By contrast, d^L describes the deviation of the total valency of the hydrons from unity; this term leads to a flattening of the correlation curve q_1 vs q_2 in the minimum. f and g are empirical numbers and may depend on the system studied.

Equation 4 provides an estimate of the *primary geometric hydrogen bond isotope effect* (primary GIE)[16]

$$\Delta q_1 = q_{1D} - q_{1H} \tag{5}$$

and of the *secondary geometric hydrogen bond isotope effect* (secondary GIE)

$$\Delta q_2 = q_{2D} - q_{2H} \tag{6}$$

The secondary effect has also been called the "Ubbelohde effect", as it was observed by this author for a number of hydrogen bonded systems.[52] It describes a different position of the heavy atoms after isotopic substitution. By contrast, the *primary geometric isotope effect* describes a different location of hydrogen isotopes in the hydrogen bond.

Equation 4 worked well in the region of strong hydrogen bonds,[20] but we noticed a numerical instability in the region of weak hydrogen bonds. In order to remove this instability, we introduced recently[53] the following changes of eq 4:

$$p_{AL} = \exp\{-(r_{AL} - r_1^\circ)/b_1\} = p_{1L}{}^* - 2d^Lp_1(p_{1L}{}^*p_{2L}{}^*)^g$$
$$p_{LB} = \exp\{-(r_{LB} - r_2^\circ)/b_2\} = p_{2L}{}^* - 2d^Lp_2(p_{1L}{}^*p_{2L}{}^*)^g$$
$$p_{1L}{}^* = p_1 - c^L(p_1p_2)^f(p_1 - p_2)$$
$$p_{2L}{}^* = p_2 + c^L(p_1p_2)^f(p_1 - p_2) \tag{7}$$

These changes removed the numerical instabilities in a satisfactory way. The new analysis was applied for the correlation of OHO hydrogen bonds.[53] The application of the above equations will be demonstrated later in the discussion.

The NMR parameters of hydrogen bonds can be related to their geometries. For example, Benedict et al. have proposed to express the chemical shifts of the nuclei of the hydrogen bridge as a function of the valence bond orders[18e]

$$\delta(A\underline{H}B) = \delta(A\underline{H})^\circ p_1 + \delta(\underline{H}B)^\circ p_2 + \Delta(A\underline{H}B)(4p_1p_2)^m$$
$$\delta(AH\underline{B}) = \delta(\underline{B})^\circ p_1 + \delta(H\underline{B})^\circ p_2 + \Delta(AH\underline{B})(4p_1p_2)^m \tag{8}$$

Here, ^{1}H chemical shifts are symbolized by underlining the letter H and ^{15}N chemical shifts by underlining the letter B. $\delta(A\underline{H})^\circ$, $\delta(\underline{H}B)^\circ$, $\delta(\underline{B})^\circ$, and $\delta(H\underline{B})^\circ$ are the limiting chemical shifts of the separate fictive groups. The terms $\Delta(A\underline{H}B)$ and $\Delta(AH\underline{B})$ represent excess hydrogen bond shifts which describe the chemical shift deviation of a symmetric or quasisymmetric complex with $p_1 = p_2 = 0.5$ from the average limiting values. m is an empirical fitting parameter with a value normally set to unity. We note that the value of $\Delta(AH\underline{B})$ might be different for equilibrium structures and structures where QZPVE is taken into account.

Equation 8 is visualized in Figure 2a for the proton of an AHB ≡ OHN hydrogen bond and in Figure 2b for the corresponding ^{15}N nucleus. For the calculation of the curves, parameters of the OHN hydrogen bonds were used, which will be discussed later. We have plotted $\delta(A\underline{H}B)$ and $\delta(AH\underline{B})$ as a function of q_1. In the strong hydrogen bond regime, when q_2 exhibits a minimum and $q_1 \approx 0$, $\delta(A\underline{H}B)$ experiences a maximum; for the weaker hydrogen bonds, $\delta(A\underline{H}B)$ changes almost linearly with q_1 and becomes constant eventually. By contrast, around $q_1 \approx 0$, $\delta(AH\underline{B})$ changes almost linearly with q_1, whereas the changes are smaller for the weaker hydrogen bonds.

RESULTS

In this section, we describe the results of our NMR studies of solid 4-MPPCP as a function of the deuterium fraction in the mobile proton site. Some data are reported for solid samples exhibiting PCP/4-MP ratios larger than 1. For a later discussion of the influence of the environment on the hydrogen bond of 4-MPPCP, we start with some liquid state NMR results obtained for polar solution.

NMR Spectroscopy of 4-MPPCP in Polar Solution. In Figure 3 are depicted some low-temperature ^{1}H and ^{15}N NMR spectra of sample **a1** containing a solution of 4-MPPCP in CDF_3/CDF_2Cl. Down to about 150 K, fast proton and

dx.doi.org/10.1021/jp305863n | J. Phys. Chem. A 2012, 116, 11370−11387

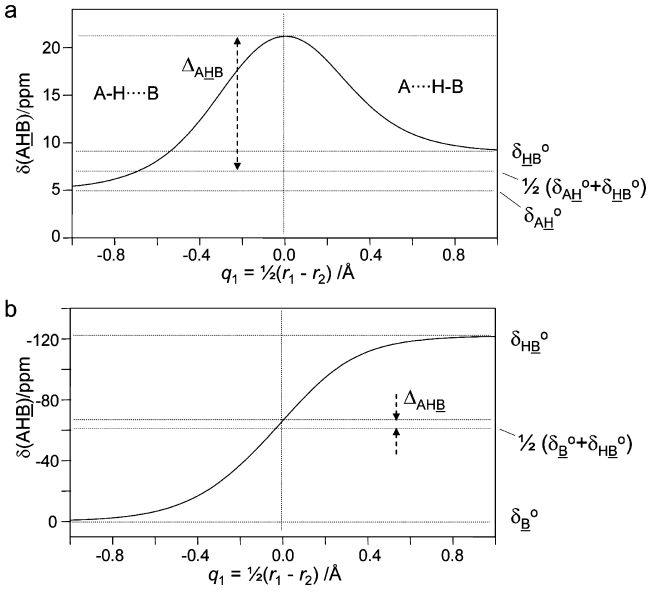

Figure 2. Chemical shifts of AHB hydrogen bonds as a function of the proton coordinate q_1 calculated using eq 8 and the parameters of Tables 3 and 4, typical for OHN hydrogen bonds between carboxylic acids and pyridine. (a) ^{1}H chemical shifts referenced to tetramethylsilane. (b) ^{15}N chemical shifts referenced to the value of the neat base.

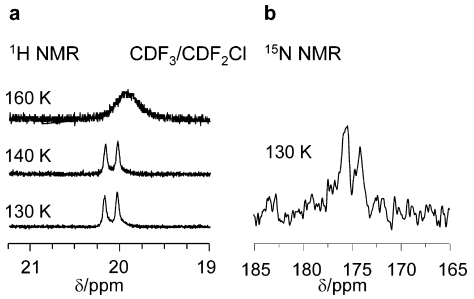

Figure 3. Low-temperature liquid state ^{1}H (a) and ^{15}N (b) NMR signals of the 1:1 complex of 4-MP with PCP in CDF_3/CDF_2Cl. ^{1}H frequency 500.13 MHz, ^{15}N frequency 50.68 MHz. Reference: solid $^{15}NH_4Cl$.

hydrogen bond exchange prevents the determination of intrinsic NMR parameters of the hydrogen bond of 4-MPPCP. At 160 K, the signal of the hydrogen bond proton gives rise to a broad line at 19.9 ppm. As the temperature is further lowered, a small low-field shift to 20.08 ppm and a decoalescence into a doublet is observed, arising from scalar one-bond coupling with the adjacent ^{15}N nucleus of 4-MP. The corresponding ^{15}N doublet is observed at 175 ppm with respect to external $^{15}NH_4Cl$ at 130 K. Because of solubility problems, the liquid state studies were not pursued further. All NMR parameters depended slightly on temperature and are assembled in Table 2.

NMR Spectroscopy of Solid 4-MPPCP. In order to characterize solid 4-MPPCP in more detail by NMR, we performed 90° pulse solid state ^{1}H, ^{2}H, and ^{15}N MAS NMR experiments on ^{15}N labeled 4-MPPCP-d_x at deuterium fractions x = 0, 0.05, 0.45, 0.7, and >0.95. As we performed the experiments at 14 T, fast MAS was required in order to average orientation-dependent nuclear interactions. We used spinning frequencies of the order of 12−18 kHz. This worked well for the ^{1}H and ^{2}H experiments, but problems arose in the ^{15}N

Table 2. NMR Parameters of the 1:1 Complex Dissolved in CDF_3/CDF_2Cl (5:1)

T (K)	signal	$\delta(^1H)$ (ppm)	$^1J(^1H,^{15}N)$ (Hz)	$\delta(^{15}N)^a$ (ppm)	$\delta(^{15}N)^b$ (ppm)	$\delta(^{15}N)^c$ (ppm)
160	singlet	19.9				
140	doublet	20.08	−68			
130	doublet	20.08	−72	−86	−91	175

[a]Referenced to 4-MP in CDF_3/CDF_2Cl (5:1). [b]Referenced to frozen 4-MP resonating at 266 ppm. [c]Referenced to solid $^{15}NH_4Cl$.

MAS experiments. We found out that ^{1}H decoupling did not enhance the resolution. This effect was studied and exploited in a later stage of this study, as will be described below. We also found out that cross-polarization (CP) and 90° pulse ^{15}N experiments gave similar signal-to-noise ratios in a given amount of time. Therefore, also in order to measure correct ^{15}N signal intensities, we performed ^{15}N MAS experiments without CP and ^{1}H decoupling. All NMR parameters obtained are assembled in Table 1.

We were able to reproduce the ^{1}H and ^{2}H MAS NMR spectra reported by Harbison et al.[37,39] The latter exhibit quadrupolar sideband patterns, whereas no side bands were observed in the ^{1}H MAS NMR spectra. In addition, for a comparison with pyridine-acid complexes studied previously in the liquid and solid states[20] and in order to determine the primary H/D isotope effects on the hydron chemical shifts, we calibrated the latter as careful as possible as described in the Materials and Methods.

In Figure 4 are depicted the ^{1}H MAS NMR spectra, the centerband ^{2}H MAS NMR spectra, and the ^{15}N MAS NMR

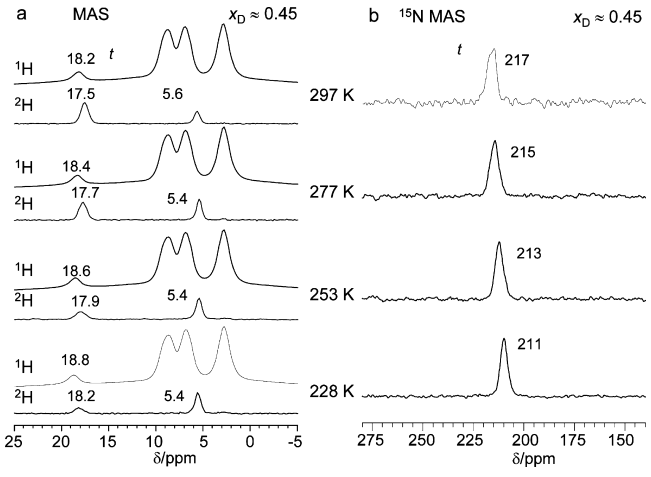

Figure 4. Temperature-dependent solid state MAS NMR spectra of sample **c** exhibiting a deuterium fraction of x_D = 0.45. (a) One-pulse ^{1}H and ^{2}H MAS NMR spectra (2.5 mm rotors, 16 kHz spinning speed). (b) 90° pulse ^{15}N MAS NMR spectra (2.5 mm rotors, 18 kHz spinning speed).

spectra of triclinic (t) ^{15}N labeled 4-MPPCP-$d_{0.45}$ (sample **c**) containing a deuterium fraction of x_D = 0.45.

All signals are sharp, indicating that MAS removes all dipolar interactions. We find a chemical shift δ(OHN) = 18.2 ppm at 297 K for the hydrogen bond proton and 17.5 ppm for the corresponding deuteron, i.e., a primary H/D isotope effect

$$^p\Delta\delta(D) \equiv \delta(OD\underline{N}) - \delta(OH\underline{N}) \quad (9)$$

dx.doi.org/10.1021/jp305863n | J. Phys. Chem. A 2012, 116, 11370−11387

of −0.7 ppm. The value of $\delta(\underline{O}H\underline{N})$ compares well with the value of 17.9 ppm given by Harbison et al.,[37,39] measured with respect to solid dimethyl sulfone-d_6, which was assumed to resonate 2.4 ppm downfield from TMS. In agreement with these authors, $\delta(^1H)$ and hence $\delta(^2H)$ increase slightly when temperature is reduced. Here, we find that $^P\Delta\delta(D)$ is reduced to about −0.6 ppm at 228 K. We also note the large difference of about 1 ppm between $\delta(\underline{O}H\underline{N})$ in the solid state and in polar solution. We assign the ^2H signal around 5.4 ppm to a small excess of the phenol; a similar excess could be present also in the ^1H spectra, where it is, however, masked by the aromatic proton signals. In Figure 4b are depicted the 90° pulse ^{15}N NMR spectra of sample **c**. Only a single band is observed at 217 ppm at 297 K which shifts slightly to 211 ppm when the temperature is lowered down to 228 K.

As depicted in the Supporting Information, deuteration does not significantly affect the ^1H and ^2H spectra, besides the ratio of the signal intensities of the hydrogen bond proton and the CH protons. By contrast, the ^{15}N signal at $x_D = 0$ (Figure S5b, Supporting Information) is sharper than that at $x_D = 0.45$ (Figure 4b). Later, we will assign this difference to a secondary one-bond isotope effect on the ^{15}N chemical shifts

$$^1\Delta\delta(N) \equiv \delta(O\underline{D}N) - \delta(O\underline{H}N) \quad (10)$$

Figure 5 shows the results of our measurements performed on fully deuterated 4-MPPCP-$d_{0.95}$. Because of the isotopic

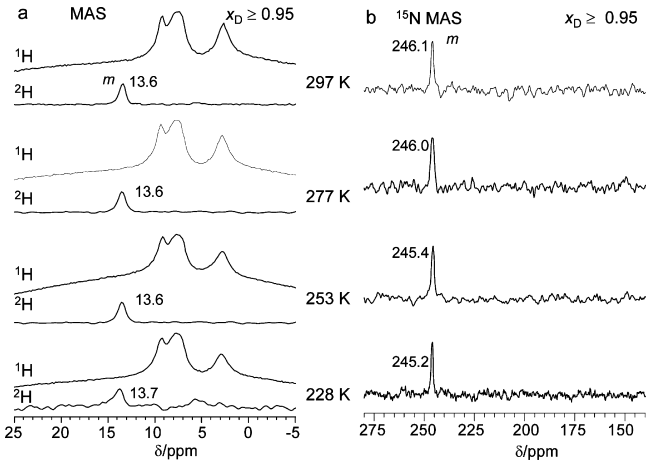

Figure 5. Temperature-dependent solid state MAS NMR spectra of sample **e** exhibiting a deuterium fraction of $x_D \geq 0.95$. (a) One-pulse ^1H and ^2H MAS NMR spectra (2.5 mm rotors, 18 kHz spinning speed). (b) 90° pulse ^{15}N MAS NMR spectra (2.5 mm rotors, 18 kHz spinning speed).

polymorphism, this sample exhibits a monoclinic (m) crystal structure.[29,37] At this deuterium fraction, Harbison et al.[37,39] observed two weak ^1H peaks around 12 and 14 ppm which were assigned to monoclinic 4-MPPCP. Here, we observe only a single ^2H peak at 13.6 ppm. In the next section, we will show that the 12 ppm peak arises from a 1:2 complex which is sometimes present in small concentrations. Because of the large deuteration fraction, no ^1H peak is observed for the hydrogen bonded protons. A sharp ^{15}N signal appears at 246 ppm. We note that both the ^2H and the ^{15}N signals of the monoclinic form do not change with temperature, in contrast to the ^1H, ^2H, and ^{15}N signals of the triclinic form.

The most interesting and unexpected spectra depicted in Figure 6 were obtained for 4-MPPCP-$d_{0.7}$ at an intermediate

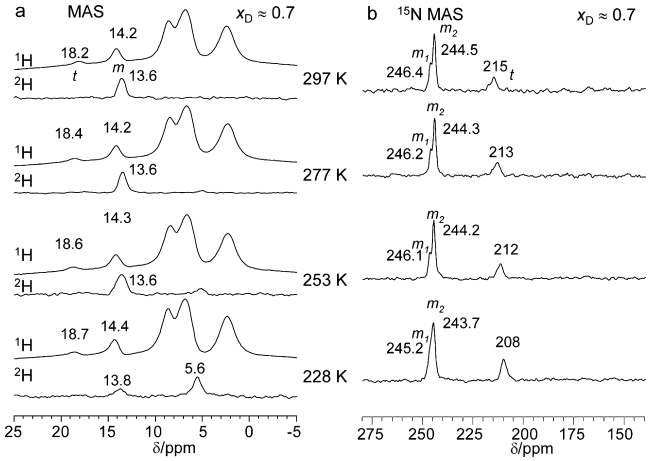

Figure 6. Temperature-dependent solid state MAS NMR spectra of sample **d** exhibiting a deuterium fraction of $x_D = 0.7$. (a) One-pulse ^1H and ^2H MAS NMR spectra (2.5 mm rotors, 16 kHz spinning speed). (b) 90° pulse ^{15}N MAS NMR spectra (2.5 mm rotors, 18 kHz spinning speed).

deuterium fraction of 0.7. The ^{15}N spectra now exhibit two peaks arising from the triclinic and monoclinic environments. The triclinic peak (t) appears at 215 ppm as at low deuterium fractions; the low-field shoulder arising from triclinic ODN bonds is almost gone. By contrast, the monoclinic signal exhibits two peaks, a smaller one (m_1) at 246 ppm, observed already for the fully deuterated sample, and a larger one (m_2) at 244 ppm. Therefore, we assign m_1 to 100% deuterated monoclinic ODN species and m_2 to monoclinic ODN species containing some OHN hydrogen bonds nearby.

This interpretation is supported by the ^1H and ^2H NMR spectra. The latter show that almost all deuterons are located in a monoclinic environment, exhibiting a chemical shift of 13.6 ppm. By contrast, OHN hydrogen bonds are observed both in the triclinic environment (18.2 ppm) as well as in the monoclinic environment, where they resonate at 14.2 ppm. This means that the monoclinic environment exhibits a primary H/D isotope effect of $^P\Delta\delta(D) = \delta(O\underline{D}N) - \delta(O\underline{H}N) = -0.6$ ppm at 297 K. One would then also expect a secondary isotope effect on the ^{15}N chemical shifts of the isotopically mixed monoclinic phase m_2, but we were not able to directly resolve the corresponding ODN and OHN signals.

^{15}N NMR Line Shape Analysis of Solid 4-MPPCP. In order to corroborate the above assignments and to estimate the secondary one-bond isotope effect on the ^{15}N chemical shifts of $^1\Delta\delta(N) = \delta(O\underline{D}N) - \delta(O\underline{H}N)$, we performed line shape analyses depicted in Figure 7. The parameters used are included in Table 1.

Figure 7a shows the analyses of triclinic peaks of sample **c** at a deuterium fraction of 0.45. This value was used to fit the spectra at all temperatures. In addition, the line widths were adapted but kept constant. Only the signal positions were adapted at each temperature. The results indicate that $^1\Delta\delta(N)$ is about +3 ppm at room temperature and decreased slightly upon cooling. A similar simulation was performed for the triclinic peaks of sample **d**, as depicted in Figure 7c, using the chemical shifts and line widths of Figure 7a as starting parameters.

Finally, we analyzed the ^{15}N signal of the monoclinic species, as depicted in Figure 7b. The mole fractions of all environments were obtained as listed in Table 1, taking into

dx.doi.org/10.1021/jp305863n | J. Phys. Chem. A 2012, 116, 11370−11387

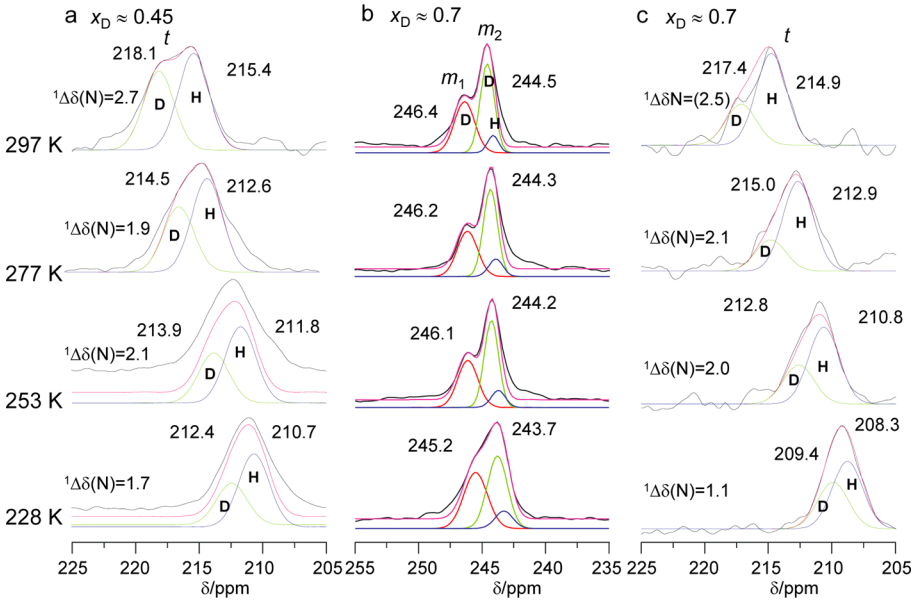

Figure 7. Superimposed experimental and calculated ^{15}N MAS NMR signals of 4-MPPCP. (a) Triclinic sample **c**, x_D = 0.45 (Figure 4b). (b) Monoclinic and (c) triclinic regions of sample **d**, x_D = 0.7 (Figure 6b). For further explanation, see the text.

account the intensity ratios of the three major peaks, i.e., 0.25 for *t*, 0.24 for m_1, and 0.5 for m_2, as well as the total deuterium content of 0.7. Assuming that the deuterium fraction in the triclinic environment is not larger than 0.04, it allowed us then to estimate the values of 0.08 of H and of 0.42 of D in m_2. These values were used for the line shape analyses of Figure 7b and c.

Recoupling of Chemical Shielding and Dipolar $^1H-^{15}N$ Coupling Tensors under $\{^1H\}-^{15}N$ Spin Decoupling. At this stage of our study, we wondered whether we could obtain additional support for the assignment of the ^{15}N signals to OHN and ODN hydrogen bonds. In fact, we obtained such a support by performing systematic ^{15}N CPMAS experiments in the presence of $\{^1H\}-^{15}N$ spin decoupling. We exploited here the second-order recoupling of chemical shielding and dipolar coupling tensors under spin decoupling which has been described for isolated heteronuclear ^1H-X two-spin systems.[54,55] As we could not find examples in the literature where larger spin systems have been studied, we were skeptical in the beginning that we could exploit this effect in the case of 4-MPPCP, which represents with the hydrogen bond proton a spin system consisting of eight protons and one ^{15}N spin. A look at the crystal structure[26] indicated that the protons of two adjacent 4-MP units are separated at least by 5 Å, corresponding to dipolar couplings below 1 kHz. Thus, we wondered whether combined ^1H decoupling and MAS would also in this case of an isolated 9-spin system exhibit the above-mentioned recoupling effects.

Indeed, such effects were observed in the $\{^1H\}$ decoupled ^{15}N CPMAS spectra depicted in Figure 8. At a deuterium fraction of x_D = 0, upon increasing the decoupling strength, the sharp signal of triclinic 4-MPPCP broadens and rapidly splits into a broad doublet, exhibiting two subsignals of equal intensity. Further increase of the decoupling strength sharpens the lines and reduces gradually the splitting, as has been described previously for isolated $^1H-^{15}N$ pairs[54] and $^1H-^{31}P$ pairs.[55] In principle, it is possible to obtain the $^1H-^{15}N$ distance from such measurements, but for that, the theory of recoupling

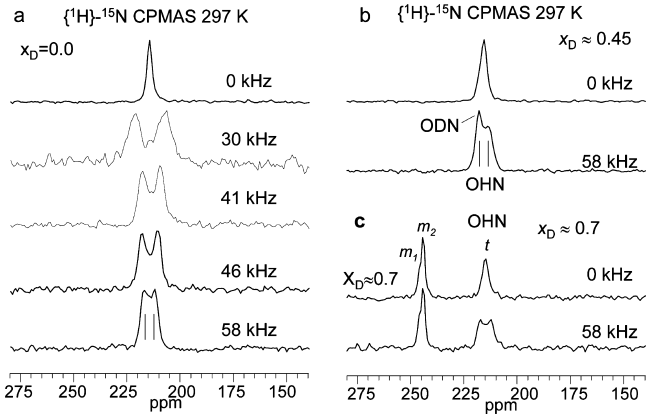

Figure 8. $\{^1H\}$ decoupled ^{15}N CPMAS NMR spectra of 4-MPPCP at different decoupling strengths (in kHz) and at different deuterium fractions in the mobile proton sites. (a) Sample **a**, x_D = 0. (b) Sample **c**, x_D = 0.45. (c) Sample **d**, x_D = 0.7. (4 mm rotors, 12 kHz spinning speed, 297 K).

in a 9-spin system needs to be developed which was outside the scope of the present study.

How could we use then this observation in order to support the signal assignment to OHN and ODN bridges of the samples containing higher deuterium fractions x_D in the hydrogen bridges? In Figure 8b are depicted the ^{15}N CPMAS spectra of the sample with x_D = 0.45 with and without $\{^1H\}$ decoupling. We observe now again a splitting in two subcomponents, but the left component is more intense than the right component. This clearly indicates that the left signal component represents a superposition of a singlet of ODN which is not affected by the recoupling, and of a symmetric doublet arising from OHN as in Figure 8a. Because of the cross-polarization, the signal of ODN might be somewhat reduced as compared to the corresponding spectrum in Figure 4b taken using single pulses.

Interestingly, at x_D = 0.7 (Figure 8c), the doublet splitting of the triclinic signal was again symmetric. This supports our

dx.doi.org/10.1021/jp305863n | J. Phys. Chem. A 2012, 116, 11370−11387

analysis above that at this deuterium fraction there is only a small amount of ODN bonds in the triclinic environment.

Precipitates of 4-MPPCP with Excess of PCP. During our initial sample preparations, when we dried the samples *in vacuo*, we observed additional signals in the solid state ^{1}H and ^{15}N NMR spectra which did not arise from the 1:1 complex between 4-MP and PCP. In order to assign these signals, we prepared solutions of 4-MP with an excess (1:2) of PCP in CH_3OH and CH_3OD, removed the solvent *in vacuo* (procedure C), and studied the resulting solid samples by solid state NMR.

The results are depicted in Figure 9. In the case of the nondeuterated sample **f**, we observed in the ^{15}N CPMAS NMR

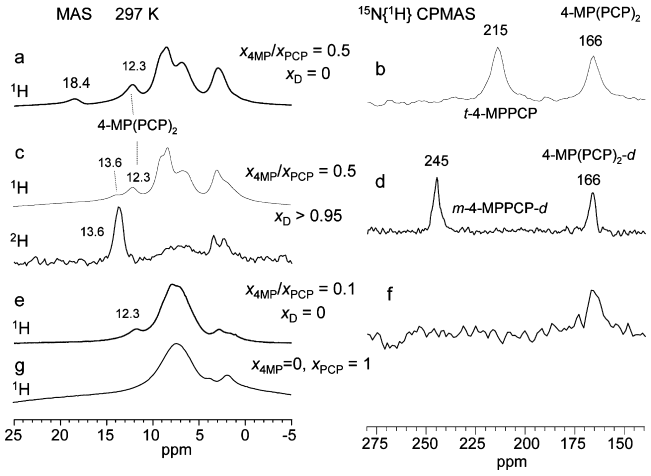

Figure 9. NMR spectra of solid samples of 4-MP containing PCP in excess. (a) One-pulse ^{1}H MAS (16 kHz spinning speed) and (b) $\{^{1}H\}$ decoupled ^{15}N CPMAS NMR spectra (30.43 MHz, 6 kHz spinning speed) of sample **f** containing a 2-fold excess of PCP as compared to 4-MP. (c) Corresponding one-pulse ^{1}H and ^{2}H MAS NMR spectra of sample **g** containing a deuterium fraction larger than 0.95 (2.5 mm, 16 kHz spinning speed). (d) ^{15}N CPMAS NMR spectra (60.8 MHz, 16 kHz spinning speed) of sample **g**. (e and f) Corresponding ^{1}H (2.5 mm, 16 kHz spinning speed) and ^{15}N (30.43 MHz, 6 kHz spinning speed) spectra of sample **h** containing a large excess of PCP. (g) One-pulse ^{1}H MAS NMR spectrum (2.5 mm, 16 kHz spinning speed) of pure PCP (sample **i**).

spectrum a signal at 166 ppm besides the signal of the triclinic 1:1 complex 4-MPPCP at 215 ppm. A similar observation was made in the ^{1}H MAS spectra which contained a signal at 12.3 ppm in addition to the signal of triclinic 4-MPPCP at 18.4 ppm. We note that the 12.3 ppm signal was observed previously by Harbison et al.[37] with a very low intensity which could, however, not be assigned at that time. We assign the new signals to complexes of the type 4-MP$(PCP)_n$ present in a different solid domain than the triclinic 1:1 complex 4-PMPCP. The high-field shift of 166 ppm clearly indicates a shift of H toward N. For $n = 2$, we propose the structure depicted in Scheme 2.

A similar observation was made for the deuterated sample **g**. The only difference is that instead of the triclinic 1:1 complex

Scheme 2. Zwitterionic 1:2 Complex 4-MP$(PCP)_2$

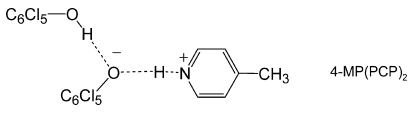

now the monoclinic 1:1 complex is present resonating at 245 ppm. By contrast, no isotope effect is observed within the margin of error for 4-MP$(PCP)_n$, giving again rise to a ^{15}N signal at 166 ppm and a ^{1}H signal at 12.3 ppm. In the ^{2}H spectra, only the peaks of monoclinic 4-MPPCP are clearly identified, whereas the 12.3 ppm signal of 4-MP$(PCP)_n$ is difficult to assign. By contrast, a broad peak was observed between 5 and 10 ppm. In order to assign this peak, we studied the ^{1}H MAS and the ^{15}N CPMAS NMR spectra of sample **h** containing a 10-fold excess of PCP, as well as the ^{1}H MAS NMR spectra of pure PCP (sample **i**). The results are depicted in Figure 9e and f. Although the ^{15}N signal is broadened, it is not shifted as compared to samples exhibiting a smaller excess of PCP. The broad ^{1}H signal between 5 and 10 ppm is clearly assigned to phenol hydrogen bonded to other phenols.

■ DISCUSSION

Using ^{1}H, ^{2}H, and ^{15}N MAS NMR, we have studied solid phases of 4-methylpyridine (4-MP) hydrogen bonded to pentachlorophenol (PCP) as a function of temperature, sample composition, and the deuterium fraction in the mobile proton sites. The ^{15}N NMR experiments confirmed the isotopic polymorphism of 4-MPPCP observed previously by X-ray crystallography[29] and by $^{1}H/^{2}H$ MAS NMR.[37,39] At a deuterium fraction of $x_D < 0.5$ in the mobile proton site, only a triclinic phase structure is observed, exhibiting a very strong OHN hydrogen bond with a O···N bond length of 2.534 Å, representing a solid solution of OHN and ODN hydrogen bonds. By contrast, at $x_D > 0.5$, a monoclinic phase appears, exhibiting a O···N bond length of 2.628 Å,[29] containing mostly ODN bonds, whereas the OHN bonds remain in the triclinic phase.

For the strong OHN hydrogen bond of the triclinic phase, we were able to determine the "primary" H/D isotope effects on the hydron chemical shifts as well as the "secondary" H/D isotope effects on the ^{15}N chemical shifts. Whereas the latter have been observed previously[12,20b] for other pyridine-acid derivatives in the solid and the liquid state, we are not aware of the determination of primary effects by solid state NMR to date.

As mentioned in the Introduction, this discussion is organized in two parts. In the first part, we correlate the NMR parameters of the OHN and ODN hydrogen bonds of triclinic and monoclinic 4-MPPCP and related complexes in the solid state and in solution with the corresponding hydrogen bond geometries, using a single hydrogen bond approach which is strictly valid only for the gas phase and liquid or solid solutions. Thus, at this stage, interactions between different hydrogen bonded complexes are not considered. In the second part, we show that such interactions, in particular the coupling of adjacent pairs of hydrogen bonds in triclinic 4-MPPCP, need to be considered in order to understand its isotopic polymorphism, the solution-solid state and temperature effects on the hydrogen bond properties of pyridine-acid complexes.

Properties of OHN and ODN Hydrogen Bonds of 4-MPPCP and Related Acid–Base Complexes. *Geometric OHN Hydrogen Bond Correlations.* In a first step, we have updated in Figure 10 various geometric correlations for OHN hydrogen bridges.[20b] The parameters used to describe the solid and dotted correlation lines are assembled in Table 3. Figure 10a contains the geometric OHN hydrogen bond correlation q_2 vs q_1. For a linear hydrogen bond, $q_2 = r_1 + r_2$ corresponds to the heavy atom distance and the proton coordinate $q_1 = {}^{1}/_{2}(r_1$

dx.doi.org/10.1021/jp305863n | J. Phys. Chem. A 2012, 116, 11370–11387

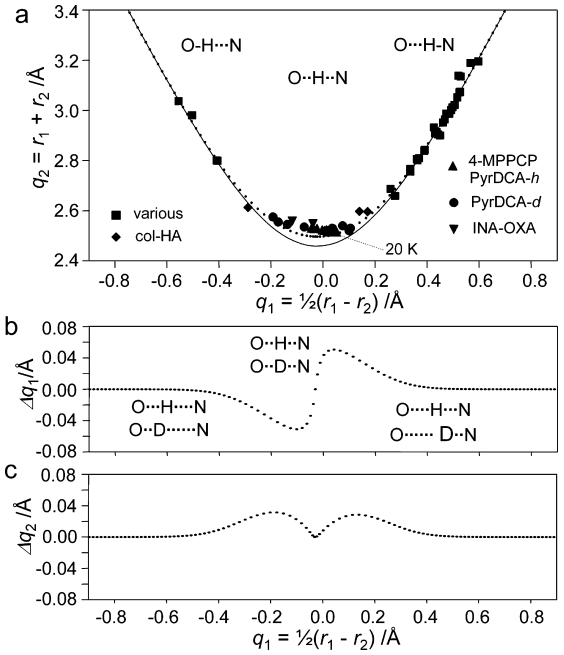

Figure 10. OHN hydrogen bond correlations. The parameters of the calculated curves are listed in Table 3. (a) Geometric OHN hydrogen bond correlation. The squares refer to various neutron diffraction data of OHN hydrogen bonded complexes in the Cambridge Structural Database as published by Steiner.[28,22] The triangles represent the neutron diffraction data of triclinic 4-MPPCP[28] and of 3,5-pyridine-dicarboxylic acid-*h*,[32] the circles to 3,5-pyridine-dicarboxylic acid-*d*,[32] the inverse triangles to the neutron structure of the pyridine-carboxylic acid OHN hydrogen bonds of isonicotinamide-oxalic acid isomorphs INA-OXA.[31] The diamonds correspond to data obtained by dipolar NMR of crystalline collidine-acid complexes.[12] (b) Estimated *primary* geometric isotope effects Δq_1 (eq 5) and (c) *secondary* geometric isotope effects Δq_2 (eq 6). Adapted from ref 20.

$- r_2$) to the distance of H from the hydrogen bond center. The data points on the left wing correspond to those complexes where H is located near oxygen. When H is shifted to and through the hydrogen bond center, the O···N distance contracts and widens again. Thus, the values of the heavy atom coordinate q_2 exhibit a minimum near $q_1 = 0$. The filled squares stem from low-temperature neutron structures of various crystals exhibiting OHN hydrogen bonds as reported by Steiner.[22] The data points of 4-MPPCP of Figure 1 obtained by Steiner et al.[28] are included as solid triangles at the bottom of the curve, together with those of 3,5-pyridine-dicarboxylic acid-*h* (PyrDCA-*h*) which have been reported recently.[32] By contrast, the data points of the deuterated analogue, PyrDCA-*d*, symbolized by circles, exhibit very different geometries, although located close to the dotted correlation line. The inverse solid triangles represent the geometries of the pyridine-carboxylic acid OHN hydrogen bonds of isonicotinamide-oxalic acid isomorphs (INA-OXA).[31] The data represented by the solid diamonds were calculated using the NH distances of collidine-acid complexes obtained by dipolar ^{2}H−^{15}N NMR[12,20b] and the N···O distance from X-ray crystallography,[56] assuming a linear OHN hydrogen bond. The neutron and NMR data sets are in good agreement with each other.

The solid line corresponds to equilibrium distances where the location of H is described in terms of a single pair of coordinates q_1 and q_2. Anharmonic quantum zero point vibrational effects (QZPVE) or other effects which are responsible for large thermal displacement ellipsoids as illustrated in Figure 1c are not taken into account. As described in the Materials and Methods section, the dotted correlation line includes a correction for QZPVE. Because of the delocalization of H, the shortest O···N distance cannot be realized. Therefore, the average values of q_2 around $q_1 = 0$ are located above the minimum equilibrium value of q_2.

The empirical correction was adjusted in such a way that the data point of 4-MPPCP derived from its neutron structure at 20 K (Figure 1b) is correctly located on the dotted correlation line. The data points corresponding to higher temperatures are located to a very small extent above this line, illustrating that upon temperature increase H is shifted through the H-bond center, accompanied by an increase of the O···N distance, slightly away from the dotted correlation curve.

The dotted curves in Figure 10b and c provide estimates of the *primary* geometric H/D isotope effects $\Delta q_1 = q_1(\mathrm{ODN}) - q_1(\mathrm{OHN})$ and the *secondary* geometric isotope effects $\Delta q_2 = q_2(\mathrm{ODN}) - q_2(\mathrm{OHN})$ (see eqs 5 and 6) as a function of the proton location q_1. The parameters *c* and *d* used (Table 3) to calculate the curves were chosen to reproduce the isotope effects on NMR chemical shifts discussed later.

In order to assist the interpretation of these curves, we have illustrated in Figure 11 two reaction pathways of hydron

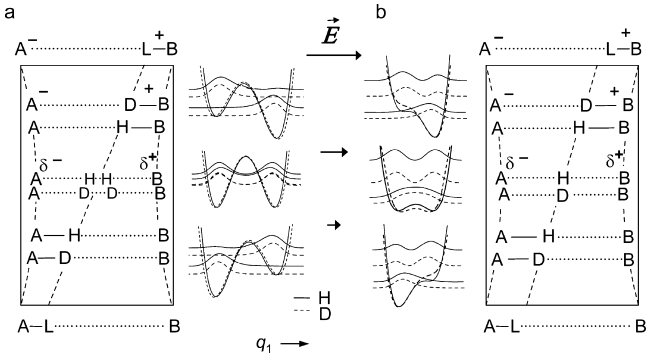

Figure 11. One-dimensional hydron (L = H, D) potentials and geometric changes during the transfer of a hydron from A to B characterized by the reaction coordinate q_1. The squares of the wave functions of the two lowest vibrational groundstates for H and D are included. (a) A barrier at the quasi-symmetric midpoint leads to a small H/D isotope effect on the geometry absent in case (b) with a very low barrier. Adapted from ref 18b.

transfer in an AHB hydrogen bond from A to B, one exhibiting a small and the other a very low or no barrier in the quasi-symmetric configuration around $q_1 = 0$. Examples of one-

Table 3. Parameters of the Geometric Hydrogen Bond Correlations of OHN Hydrogen Bonds in Pyridine−Acid Complexes

	b_{OH}[a] (Å)	$r_{OH}°$[a] (Å)	b_{HN}[a] (Å)	$r_{HN}°$[a] (Å)	*f*	*g*	c^H	d^H	c^D	d^D
OHN	0.371	0.942	0.385	0.992	5	2	360	0.45	30	0.45

[a]Taken from ref 22. The other values are taken from ref 20b.

dx.doi.org/10.1021/jp305863n | J. Phys. Chem. A 2012, 116, 11370−11387

dimensional potential curves calculated using known procedures[57] illustrate schematically different configurations along the pathways. Squares of the lowest vibrational wave functions for H and D are included. In principle, more-dimensional surfaces have to be used for a quantitative description.[11,18,58]

In the case of weak hydrogen bonds, deuteration exhibits little effects. When the hydron position is shifted toward the hydrogen bond center, deuteration shortens the "covalent" bond and lengthens the "hydrogen bond" in the case of both pathways. This is illustrated by the different positions of the maxima of the H and D distribution functions, corresponding to the squares of the vibrational wave functions depicted in the upper and lower parts of both Figure 11a and b. Negative values of the primary geometric isotope effect Δq_1 result as illustrated in Figure 10b when H is close to A and positive values when H is close to B. The correlation curve Δq_1 vs q_1 exhibits then a dispersion-like shape. By contrast, Δq_2 is positive in both wings, leading to a camel-like shape of the correlation curve for the secondary geometric isotope effect Δq_2 vs q_1, as depicted in Figure 10c.

At the quasi-symmetric configuration around $q_1 = 0$, the primary geometric isotope effect $\Delta q_1 = 0$ both in Figure 11a and b. By contrast, Δq_2 depends on the barrier height. If the barrier is very small or absent, D is more confined on average to the hydrogen bond center than H, leading to a negative value of Δq_2, as illustrated in Figure 11b.[59] By contrast, for a larger barrier, H is more confined to the hydrogen bond center as compared to D, and a positive value results, as illustrated in Figure 11a. In Figure 10c, we have assumed that the barrier height is such that $\Delta q_2 = 0$ at the quasi-symmetric configuration.

Finally, in Figure 11, we have assumed that AHB represents a neutral complex which becomes zwitterionic when H is shifted from A to B. This shift can occur if the acidity of AH is increased, but also when AHB is placed in the electric field.[11,60] Thus, these hydrogen bonds are "easily polarizable", as has been demonstrated by Zundel et al.[61] In condensed matter, the interaction with neighboring molecules then can lead to similar effects, as discussed below.

NMR Hydrogen Bond Correlations. As information about hydrogen bond geometries cannot be obtained easily by diffraction techniques in the case of liquids and biosystems, the question arises whether such information can be obtained by a discussion of chemical shifts. For OHN hydrogen bonds in pyridine-acid complexes, a link between ^{15}N NMR chemical shifts $\delta(\mathrm{OH\underline{N}})$ and hydrogen bond geometries has been found,[12] as illustrated in Figure S7a of the Supporting Information and applied to cofactor-protein interactions.[17] In addition, a correlation of H-bond geometries with the hydron chemical shifts $\delta(\mathrm{O\underline{H}N})$, with the *primary* isotope effects on the hydron chemical shifts $^{\mathrm{P}}\Delta\delta(\mathrm{D})$ (eq 8) and with the *secondary* H/D isotope effects on the nitrogen chemical shifts, was observed.[20a]

Updated correlation diagrams which include the data of 4-MPPCP are illustrated in Figure 12. In order to facilitate the comparison between different pyridine-acid complexes, and to minimize structural effects, the values of $\delta(\mathrm{OH\underline{N}})$ are referenced individually to those of the corresponding neat frozen bases assembled in Table 4; i.e., we set $\delta(\underline{\mathrm{N}})^\circ = 0$ in eq 8 used to calculate the dotted correlation curve of Figure 12a where we have plotted the ^{1}H chemical shifts $\delta(\mathrm{O\underline{H}N})$ of hydrogen bonded 1:1 complexes of ^{15}N labeled pyridine derivatives with various acids as a function of their ^{15}N chemical shifts $\delta(\mathrm{OH\underline{N}})$. Filled symbols refer to solid complexes measured at room temperature and open symbols to complexes measured in the temperature region between 100 and 150 K, using CDF_3/CDF_2Cl as solvent.

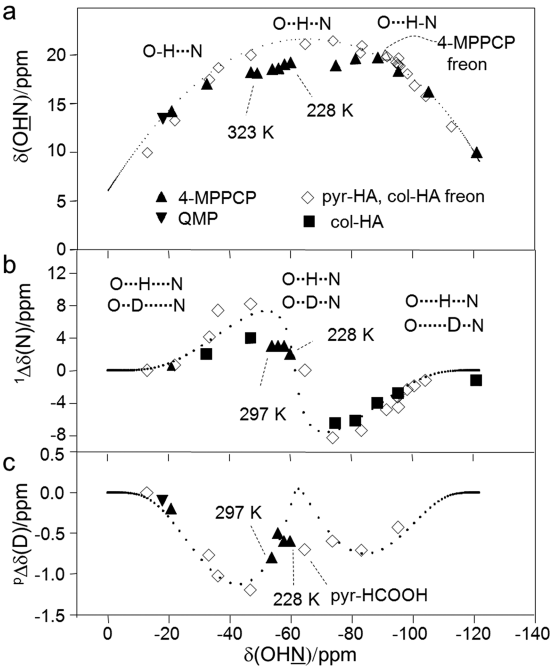

Figure 12. (a) ^{1}H vs ^{15}N chemical shift correlation of pyridine- and substituted pyridine acid complexes. (b) *Secondary* (eq 10) and (c) *primary* isotope effects (eq 9) on the ^{15}N chemical shifts $\delta(\mathrm{OH\underline{N}})$ (referenced to the neat frozen bases). The open symbols refer to solutions in CDF_3/CDF_2Cl around 130 K. The filled symbols refer to solid phases. The data of the pyridine and collidine complexes were taken from refs 12, 19, and 20b, and those of 4-MPPCP were obtained in this study. All values of $\delta(\mathrm{OH\underline{N}})$ are referenced to the neat frozen bases. QMP: quinidine-methylparaben cocrystal containing a pyridine-phenol type OHN hydrogen bond according to Khan et al.[66]

Table 4. Parameters of the NMR Hydrogen Bond Correlations of Hydrogen Bonded Complexes of Pyridine Type Bases with Acids[a]

B = pyridine	neat frozen solid[b]	$\delta(\underline{\mathrm{N}})^\circ$	275
B = pyridine	in CDF_3/CDF_2Cl around 130 K[b]	$\delta(\underline{\mathrm{N}})^\circ$	271
B = collidine	neat frozen solid around 130 K[b]	$\delta(\underline{\mathrm{N}})^\circ$	268
B = collidine	in CDF_3/CDF_2Cl around 130 K[b]	$\delta(\underline{\mathrm{N}})^\circ$	260
B = 4-methylpyridine	neat frozen solid around 130 K[b]	$\delta(\underline{\mathrm{N}})^\circ$	266
B = 4-methylpyridine	in CDF_3/CDF_2Cl around 130 K[b]	$\delta(\underline{\mathrm{N}})^\circ$	261
BH^+	all bases	$\delta(\underline{\mathrm{H}}\mathrm{N})^\circ$	9
AH	RCOOH	$\delta(\mathrm{O\underline{H}})^\circ$	6
BH^+	all bases[c]	$\delta(\mathrm{H\underline{N}})^\circ$	−122
AHB	all bases	$\Delta(\mathrm{O\underline{H}N})$	16
AHB	all bases[c]	$\Delta(\mathrm{OH\underline{N}})$	−16
AHB	all bases	$^1J(\underline{\mathrm{H}}\mathrm{N})^\circ$	110
AHB	all bases	$J(\mathrm{O\underline{H}N})^*$	12.5

[a]Chemical shifts δ in ppm, coupling constants J in Hz. [b]^{15}N chemical shifts with respect to solid $^{15}NH_4Cl$. [c]^{15}N chemical shift with respect to free base.

dx.doi.org/10.1021/jp305863n | J. Phys. Chem. A 2012, 116, 11370−11387

Let us first discuss the dotted correlation curve calculated using the NMR parameters of Table 4 defined in the Materials and Methods. The parameters were adjusted to reproduce the liquid state data which exhibit slightly larger values than the solid state data. Essentially, the parameters are similar to those reported previously.[18,20b,62]

The ^{15}N chemical shift corresponding to the strongest hydrogen bond to a pyridine derivative is shifted to about −77 ppm to high field with respect to the free neat base, whereas the arithmetic mean of the shifts of the free base and free protonated nitrogen is only −61 ppm. The difference, −16 ppm, corresponds to the excess term $\Delta(OH\underline{N})$ in eq 8 and Table 4. Previously, we did not have such precise information and neglected this term.

Another difference arises from the recent finding that it is not possible to use a single limiting ^1H chemical shift $\delta(O\underline{H})°$ of free proton donors such as carboxylic acids and alcohols, in contrast to our previous assumptions.[63,64] Whereas for the first values of 5−6 ppm seem to be appropriate, free alcohol and water absorb around 0 ppm.[53] Therefore, ^1H vs ^{15}N chemical shift correlation curves of OHN hydrogen bonds depend on the type of proton donor when H is located nearer to the acid than to the nitrogen base.

The liquid solution data in Figure 12a refer to complexes using pyridine (pyr)[18b] and collidine (col)[19] as bases. The new data point obtained here for 4-MPPCP in freon solution at 130 K (Figure 3) is characterized by a open triangle and is especially highlighted, as it is somewhat hidden behind other data points.

Whereas complexes of the pyridine-carboxylic acid type in solution reach maximum ^1H chemical shifts of about 21 ppm, the corresponding value for the solid state is about 2 ppm smaller, as illustrated by data of solid collidine-acid complexes,[12] characterized by solid squares, and the new data obtained here for solid 4-MPPCP, symbolized by filled triangles. We will discuss the origin of this effect later in more detail.

The data point characterized by a ^{15}N chemical shift of −21 ppm (with respect to neat 4-methylpyridine, 245 ppm with respect to $^{15}NH_4Cl$) corresponds to the monoclinic form at room temperature, those in the center to the triclinic form between 228 and 323 K. Data points corresponding to pyridine-water and pyridine-SiOH complexes[65] included previously in the related graph of Figure 4c in ref 20b have been omitted now, as they require a different correlation curve.

The new data set of 4-MPPCP compares well with those of the other solid complexes. Particularly interesting is the shift of the data point of 4-MPPCP when going from the solid to the polar liquid mixture CDF_3/CDF_2Cl state at 130 K, exhibiting a dielectric constant ε of about 30 at this temperature. The ^{15}N high-field shift indicates the formation of a zwitterionic form in solution. On the other hand, the ^1H signal shifts to lower field when going from the solid to the liquid. We will discuss these effects later.

In the diagram, we have included the $^1H/^{15}N$ chemical shift data of a quinidine-methylparaben cocrystal (QMP) containing a quinoline-phenol type OHN hydrogen bond published by Khan et al.[66] The hydrogen bond is relatively weak, but in spite of the different substituents, the data point is very well located on the dotted correlation curve.

We note that the data point of the 1:2 complex of 4-MP with PCP (Scheme 2 and Figure 9) is not well located on the correlation curve; we did not include this data point, as the ^1H value of 12.3 ppm may not arise from the OHN hydrogen bond but from the OHO hydrogen bond. We also note that Figure S7b (Supporting Information) illustrates how the scalar couplings $^1J(O\underline{H}N)$ between ^1H and ^{15}N correlate with $\delta(OH\underline{N})$. The value of 4-MPPCP in freon is well located on the correlation line proposed previously.[20b]

In Figure 12b and c, we have depicted the experimental H/D isotope effects $^1\Delta\delta(N)$ and $^P\Delta\delta(D)$ of pyridine-acid complexes in solution and the solid state as a function of $\delta(OH\underline{N})$. Previously, we had not been able to observe primary effects $^P\Delta\delta(D)$ for the solid state.[18b] Here, we succeeded in the case of triclinic 4-MPPCP to measure both $^1\Delta\delta(N)$ depicted in Figure 12b as well as $^P\Delta\delta(D)$ included in Figure 12c. The chemical shifts of the deuterated ODN bridges were obtained at low deuterium fractions in an environment of OHN bridges. The data points are well located on the dotted correlation curves which were calculated using the parameters included in Tables 3 and 4. These curves are analogues of those in Figure 10b and c; except for the NMR parameters, they depend on the same geometric parameters. Thus, the latter and hence the curves of Figure 10b and c were determined by adapting the dotted lines of Figure 12b and c to the experimental data.

Generally, we find that the secondary isotope effects $^1\Delta\delta(N)$ are somewhat smaller for the solid state as compared to polar solution, where the difference is larger when H is closer to oxygen than to nitrogen. The primary isotope effects $^P\Delta\delta(D)$ in Figure 12c are better located on the dotted correlation curve. An exception is the data point of the pyridine-formic acid complex in freon at 109 K. Its value deviates from the value predicted by the correlation curve. We note that similar effects are observed for the homoconjugated pyridine and collidine cations which exhibit NHN hydrogen bonds.[59,67] The deviation indicates that the shortest heavy atom distances are not reached, which may be a sign of a distribution of H-bond geometries in solution or a tautomerism between two forms. Evidence for tautomeric equilibria in pyridine-acid complexes has been obtained by Perrin et al. from the study of ^{18}O isotope effects on ^{13}C chemical shifts using dichloromethane as solvent.[68] However, by comparison with Figure 10c, it becomes clear that the q_1 values must be between −0.1 and +0.1 Å, indicating that we do not deal with the usual tautomerism between two well-defined limiting structures as typically found for intramolecular OHN hydrogen bonds.[21d]

Finally, the primary H/D isotope effect of −0.1 ppm measured for QMP by Khan et al.[66] is also well located on the dotted correlation line of Figure 12c.

Isotopic Polymorphism, Temperature Effects, and Coupling of OHN Hydrogen Bonds in 4-MPPCP. *Zero-Point Energy Differences as Potential Causes of Isotopic Polymorphism.* In this section, we discuss the isotopic polymorphism of 4-MPPCP as well as its possible origin. The overview depicted in Figure 13 indicates quite a complex behavior. In agreement with the $^1H/^2H$ NMR findings of Harbison et al.,[37,39] at deuterium fractions $x_D < 0.5$, only the triclinic form is observed. Under these circumstances, triclinic 4-MPPCP is able to incorporate ODN hydrogen bridges in an environment of OHN hydrogen bridges. At $x_D > 0.5$, ^{15}N NMR shows that the triclinic phase loses most ODN hydrogen bonds which form then the monoclinic phase *m*. *m* contains two environments labeled as m_1 and m_2. We tentatively assign m_1 to ODN hydrogen bonds surrounded by other ODN hydrogen bonds and m_2 to ODN hydrogen bonds which feel an OHN hydrogen bond nearby (Table 1).

dx.doi.org/10.1021/jp305863n | J. Phys. Chem. A 2012, 116, 11370−11387

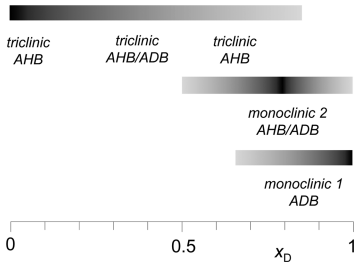

Figure 13. Isotopic polymorphism of 4-MPPCP revealed by ^{15}N solid state NMR.

The traditional way to explain isotopic equilibria is based on the theory of isotope effects developed by Bigeleisen et al.[69] H/D isotope effects on chemical equilibria arise mostly from differences in zero-point energies of hydrogenic vibrations in the different equilibrating forms.

Along this line, Harbison et al.[39] have rationalized the isotopic polymorphism of 4-MPPCP between the pure triclinic and the pure monoclinic phase depicted schematically in Figure 14a. On the basis of a vibrational analysis using inelastic

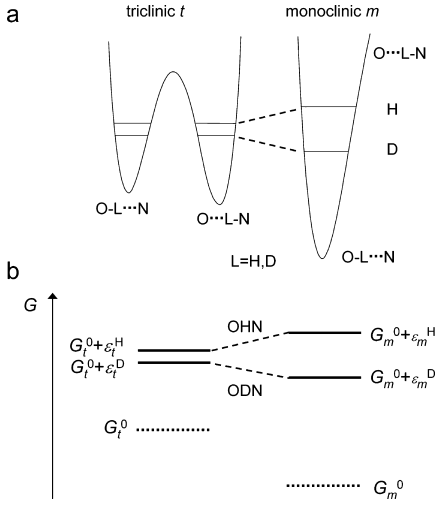

Figure 14. (a) Explanation of the isotopic polymorphism of 4-MPPCP in terms of zero-point energy differences between the triclinic and monoclinic forms according to ref 39. (b) Expansion of the energy diagram of Figure 14a into a Gibbs free energy diagram.

neutron scattering of triclinic 4-MPPCP-d_7, deuterated in the carbon positions, and IR data of monoclinic 4-MPPCP-d_1,[29] it was estimated that for the triclinic phase the zero-point energy difference $\varepsilon_t^H - \varepsilon_t^D$ of the hydrogenic H and D vibrations is very small, whereas the difference $\varepsilon_m^H - \varepsilon_m^D$ for the monoclinic form is about 500 cm^{-1}. These findings were rationalized qualitatively in terms of the one-dimensional potential curves depicted in Figure 14a. If the potential curves are arranged vertically, as shown in Figure 14a, the OHN-level goes up and the ODN-level decreases in energy when going from the triclinic to monoclinic form.

In Figure 14b, we have redrawn the diagram of Figure 14a as a Gibbs free energy G diagram. G needs to be considered instead of energy E when different phases are compared with respect to their relative stabilities. Let us define G_t° and G_m° as the "equilibrium" molar Gibbs free energy of the triclinic and monoclinic phases illustrated by the horizontal dotted lines, in which the zero-point energies ε_t^L and ε_m^L, L = H, D, of the hydrogenic vibrations are omitted. The ground states of the triclinic and monoclinic forms are then given by $G_t^\circ + \varepsilon_t^L$ and by $G_m^\circ + \varepsilon_m^L$, as illustrated in Figure 14b by the bold horizontal lines. If $G_m^\circ < G_t^\circ$, and the difference $|G_t^\circ - G_m^\circ|$ is fixed to a favorable range of values, $G_m^\circ + \varepsilon_m^H > G_t^\circ + \varepsilon_t^H$ and $G_m^\circ + \varepsilon_m^D < G_t^\circ + \varepsilon_t^D$. This can explain the observed isotopic polymorphism of 4-MPPCP taking into account the Gibbs phase rule which states that the number of phases is $P = C - F + 2 = 1$ for solids with single components $C = 1$ and $F = 2$ degrees of freedom for temperature and pressure. Therefore, in Figure 14b, only the state with the lowest free energy is considered at a given temperature and pressure; i.e., there is no Boltzmann distribution between the different phases of a pure component.

Two questions remain open. The first problem is the reason why G_m° is smaller than G_t°. The second problem is the treatment of solid 4-MPPCP at intermediate deuterium fractions x_D. If one sets the number of components $C = 2$, two phases may coincide according to the Gibbs phase rule at intermediate values of x_D, i.e., triclinic 4-MPPCP-*h* and monoclinic 4-MPPCP-*d*. On the other hand, as stated above, at $x_D < 0.5$, a triclinic solid solution is observed.

Geometric Isotope Effects and Mutual Hydrogen Bond Interactions as a Potential Cause of Isotopic Polymorphism. We offer here a solution to both problems which is based on the mutual interaction of hydrogen bonded complexes in the polymorphs and on the geometric H/D isotope effects observed. According to the packing diagram of Figure 1, the hydrogen bonded complexes of triclinic 4-MPPCP-*h* are arranged in pairs with antiparallel OHN hydrogen bonds, about 6 Å away from each other. As illustrated in Figure 15a, the protons are located near the hydrogen bond centers; thus, each complex exhibits a large electrical dipole moment. This leads to a mutual attraction and a cooperative coupling, as found previously in a number of cases.[62,63,70] Because of their proximity, the two hydrogen bridges are cooperative in the sense that they polarize each other. In triclinic 4-MPPCP, around room temperature, both H's in both bridges have just crossed the hydrogen bond center and are located on average somewhat closer to O than to N. Now, if H in the lower bridge is substituted by D (Figure 15b), the geometric isotope effects in Figures 11 and 12 indicate that D is displaced somewhat toward oxygen, accompanied by an increase of the O···N distance. This leads to a reduction of the dipole moment of the bridge. The electric field produced at the upper bridge is then reduced. As a consequence, the dipole moment of the upper bridge is also somewhat reduced, and hence H in the upper bridge exhibits also a geometric change, which is, however, smaller than in the lower bridge. Similar effects have been observed for other coupled hydrogen bonded systems by experiment and theory.[58,59] As a result, the dipole−dipole interaction is somewhat reduced, which destabilizes somewhat the triclinic form. However, this form is apparently still stable until each hydrogen bonded pair contains up to 1 deuteron, i.e., up to a deuterium fraction of about 0.5.

By contrast, when both bridges of a pair are deuterated, each hydrogen bridge becomes weaker; i.e., both O···D distances are reduced and both O···N distances are increased, as illustrated in Figure 15c. Thus, also the corresponding dipole moments are reduced. That leads to a decrease of the dipole−dipole interactions of the two adjacent hydrogen bonds and hence to an increase of the energy of the triclinic polymorph. Thus, the antiparallel arrangement is destroyed (Figure 15c) and

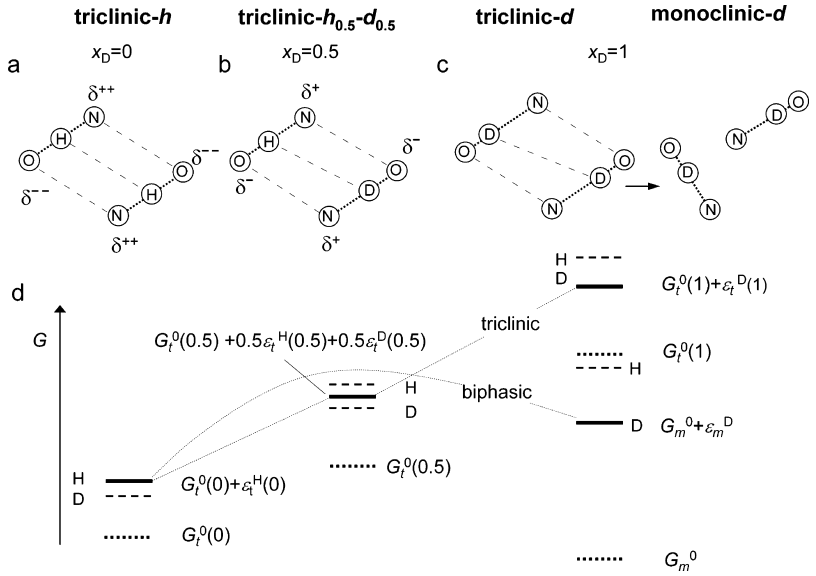

Figure 15. Origin of the isotopic polymorphism of 4-MPPCP proposed in this study. (a) Visualization of the OHN/OHN dipole−dipole interaction in triclinic 4-MPPCP-*h*. (b) Deuteration of one hydrogen bond decreases the hydron−oxygen distance and increases the hydron−nitrogen distance. The effect is somewhat transmitted to the neighboring pair. The dipole−dipole interaction is reduced but still strong enough to stabilize the triclinic structure. (c) Full deuteration leads to a lengthening of both hydrogen bonds and hence to a further reduction of the dipole−dipole interaction. The latter does not dominate the packing any more, and other intermolecular interactions such as C−H···Cl hydrogen bonds take over, leading to a different packing and hence a monoclinic structure after deuteration. (d) Schematic Gibbs free energy diagram of triclinic 4-MPPCP at deuterium fractions x_D = 0, 0.5, and 1 and of the monoclinic form at x_D = 1. The straight dashed lines represent the molar Gibbs free energies of the triclinic form at different deuterium fractions. The upward curved dashed line represents the total molar Gibbs free energy of the coexisting triclinic and monoclinic phases. For further explanation, see the text.

other interactions become dominant. In particular, the X-ray structure indicates[29] that C−H···Cl hydrogen bonds take over and dominate the packing. Now, the complexes are oriented perpendicular to each other and monoclinic crystals are formed, as illustrated in Figure 15c.

In order to explain this behavior, we have constructed the schematic Gibbs free energy diagram depicted in Figure 15d. The molar Gibbs free energies are symbolized by bold horizontal lines. Vibrational ground states whose populations depend on the deuterium fraction x_D are symbolized by horizontal dashed lines.

We assume that the "equilibrium" molar Gibbs free energy of the triclinic form increases with an increase of the deuterium fraction x_D but that the value of the monoclinic form does not significantly depend on x_D, i.e.,

$$G_t^\circ = G_t^\circ(x_D), \qquad G_m^\circ = \text{constant} \tag{11}$$

This increase is justified by the loss of dipole−dipole energy between adjacent OLN dipoles when the deuterium fraction is increased, as was discussed above. We keep the frequencies of the hydrogenic vibrations, i.e., the zero-point energies to similar values as in Figure 14. Thus, we use smaller values for the triclinic form and larger values for the monoclinic form, but their exact values are not essential. However, we take into account that the frequencies of the hydrogenic vibrations, i.e., the corresponding zero point energies, might increase somewhat in the triclinic form when the deuterium fraction is increased, whereas such changes will be small for the monoclinic form. Thus, we write

$$\varepsilon_t^{\,L} = \varepsilon_t^{\,L}(x_D), \qquad \varepsilon_m^{\,L} = \text{constant}, \qquad \text{where L} = \text{H, D} \tag{12}$$

This leads to the Gibbs free energy diagram depicted in Figure 15d. On the left-hand side, the situation of the triclinic phase at x_D = 0 is depicted, characterized by the molar Gibbs free energy of $G_t^\circ(0) + \varepsilon_t^{\,H}(0)$. After deuteration, at x_D = 1, the molar Gibbs free energy of the triclinic form has strongly increased to $G_t^\circ(1) + \varepsilon_t^{\,D}(1)$, resulting in a spontaneous transition to the monoclinic form exhibiting a much smaller value of $G_m^\circ + \varepsilon_m^{\,D}$. The preference for the monoclinic phase after deuteration is much less sensitive to the difference between $G_t^\circ(1)$ and G_m°, and to the zero-point energy differences, in contrast to the model of Figure 14.

At x_D = 0.5, the molar Gibbs free energy will be about halfway between $G_t^\circ(0)$ and $G_t^\circ(1)$. We assume that the zero-point energy contribution is given by the weighted average of the OHN and ODN hydrogen bonds, leading to a molar Gibbs free energy of $G_t^\circ(0.5) + 0.5\varepsilon_t^{\,H}(0.5) + 0.5\varepsilon_t^{\,D}(0.5)$.

The choice of values of $G_t^\circ(x_D)$ and of G_m° is such that the triclinic form is still the dominant one at x_D = 0.5, in agreement with the experiment. Only above this value, the phase separation occurs.

Finally, the question arises whether the diagram can explain why the triclinic phase separates into the triclinic-*h* and the monoclinic-*d* phases only above a deuterium fraction of x_D = 0.5. It is clear that the separation into two phases requires the mixing entropy to be overcome. In order to take this effect into account, we tentatively added to Figure 15d the dashed upward bulge curve to represent the molar Gibbs free energy of the separated phases. At x_D = 0.5, the molar Gibbs free energy increases upon phase separation, whereas at higher degrees of deuteration the biphasic mixture becomes more stable, in agreement with the results depicted in Figure 13. We note that this treatment is qualitative, and does not yet take into account the observation that in the region where the biphasic mixture is

dx.doi.org/10.1021/jp305863n | J. Phys. Chem. A 2012, 116, 11370−11387

stable, e.g., at $x_D = 0.7$, the triclinic-*h* contains a small amount of ODN and monoclinic-*d* a small amount of OHN.

Temperature and Solid–Liquid State Effects. The ^{1}H and ^{2}H NMR signals of the hydrogen bonded hydrons of triclinic 4-MPPCP exhibit a temperature shift of about $\Delta\delta/\Delta T \approx -1 \times 10^{-2}$ ppm/K and a ^{15}N shift of about $+1 \times 10^{-1}$ ppm/K. Surprisingly, within the margin of error, neither ^{2}H nor ^{15}N chemical shift changes are observed for the ODN hydrogen bond of monoclinic 4-MPPCP (Figure 5). How can the difference between the two systems be explained?

Since a long time, excitation of various hydrogen bond vibrations has been discussed to explain temperature dependent average chemical shifts of well characterized hydrogen bonded complexes in solution.[71] However, it is often difficult to separate this phenomenon from temperature dependent solvent effects. The latter are not operative in crystals; thus, recently, for the COOH proton of the polycrystalline dipeptide *β*-L-aspartyl-L-alanine, hydrogen bonded to the COO^- group of an adjacent molecule, a value of $\Delta\delta/\Delta T \approx -0.3 \times 10^{-2}$ ppm/K has been reported and explained in terms of vibrational excitation.[72] According to the OHO-bond correlations,[53] this can be explained in terms of a lengthening of the average H···O distances. However, this phenomenon alone cannot explain the different behavior of triclinic and monoclinic 4-MPPCP.

Another explanation of temperature-dependent chemical shifts of pyridine-acid complexes in solution has been proposed by some of us, based on low-temperature NMR studies using the polar freon mixture CDF_3/CDF_2Cl as solvent.[73] Its dielectric constant increases strongly from 10 at 298 K to 45 at 100 K.[74] For the molecular pyridine-acetic acid complex where H was closer to O than to N, a low field shift was observed upon decreasing temperature, with $\Delta\delta/\Delta T \approx -1.7 \times 10^{-2}$ ppm/K. The maximum chemical shift $\delta(^1H)_{max} \approx 21$ ppm was reached in the case of the very strong chloroacetic acid complex. By contrast, the H-bond proton signal of the zwitterionic pyridine-HCl complex appeared again at higher field but did not shift to high but to low field upon increasing temperature. Thus, a sign reversal of $\Delta\delta/\Delta T$ was observed, i.e., $+1 \times 10^{-2}$ ppm/K.

These findings were modeled theoretically in terms of an increase of the local electric fields at the OHN hydrogen bonds when temperature is lowered,[60,73,74] as illustrated schematically in Figure 16a. At high temperature, these fields are small because the solvent molecules are disordered. However, the fields become larger when solvent ordering occurs at lower temperatures, as indicated by the strong increase of the dielectric constant. The DFT calculations showed[60] that these fields increase the OHN dipole moments by displacing the average H positions along the geometric correlation line (Figure 10a) from O toward N. The correlation curve of Figure 12a, where the ^{15}N chemical shift is a qualitative measure of the proton position with respect to the H-bond center and the ^{1}H chemical shift a qualitative measure of the O···N distance, then explains first the low field shift of the H-bond proton and after passing through the hydrogen bond center the observed high field shifts upon lowering the temperature and increasing the proton donating power of the acid in the complex.

We propose to use a similar scenario depicted in Figure 16b to describe the temperature-dependent geometric changes of triclinic 4-MPPCP. At very low temperatures, the neutron structures (Figure 1c) indicate zwitterionic hydrogen bond pairs, where the H are located near the N (Figure 16d). At higher temperatures, vibrational excitation in one bridge will

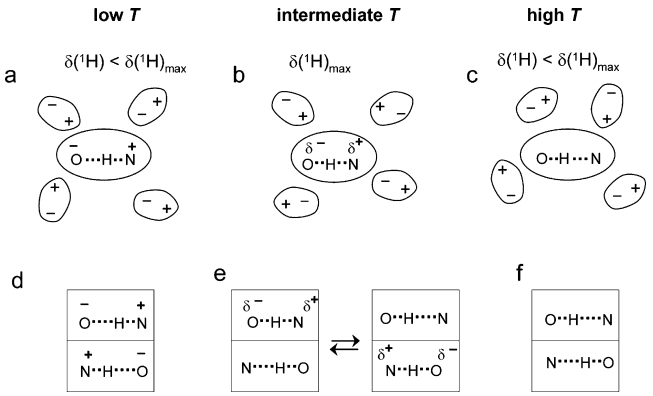

Figure 16. Temperature-dependent zwitterion formation of neutral OHN hydrogen bonded complexes and associated ^{1}H chemical shifts. (a–c) Driven by ordering of solvent dipoles at low temperatures and (d) to (f) driven by electrical dipolar couplings between two complexes oriented in an antiparallel way. For further explanation, see the text.

shift H toward the H-bond center or beyond, as one can infer from the simple models depicted in Figure 11. In a similar way as deuteration, the electric field at the neighboring H-bond will then also be reduced due to the mutual cooperative coupling, and the dipole moment decreased by shift of H toward the H-bond center. However, as the H-bond vibrations are subject to intermolecular coupling, i.e., to the formation of optical phonons, the excitation will move from one bridge to the next (Figure 16e), and even to other surrounding pairs. Thus, on average, a shift of the hydrogen bond geometry more or less along the correlation line will occur, as was illustrated by the solid triangles in Figure 12a. The reduction of the local electric fields will be pronounced at higher temperatures, and both H's will move closer to oxygen (Figure 16f). These considerations refer to the average geometries; however, the distribution of geometries increases with increasing temperature, as illustrated by the increase of the widths of the thermal displacement ellipsoids in Figure 1c. The observation that only the left edges but not the right edges of the ellipsoids change with temperature indicates that configurations with smaller dipole moments where H is located closer to oxygen are populated when the temperature is increased. This is in agreement with the finding that the electronic spectrum of triclinic 4-MPPCP contains components at 32520 and 30600 cm^{-1}, associated to contributions from a zwitterionic and a molecular form.[27]

Our interpretation is supported by the observation that temperature dependent chemical shift changes are only observed for triclinic but not for monoclinic 4-MPPCP-*d*. In the latter, two adjacent complexes are oriented perpendicular to each other where the dipole–dipole interaction is small.

Figure 16 can also explain the observed ^{15}N high-field shift of 4-MPPCP between the solid state at room temperature and polar freon solution at 130 K, as was illustrated by the corresponding data points in Figure 12a. The high-field shift indicates a substantial lowering of the H···N distance, i.e., stabilization of the zwitterionic form by the highly ordered polar solvent molecules. Similar solid–liquid state effects for other pyridine-acid complexes have been observed previously.[19]

Maximum ^{1}H Chemical Shifts. Let us now discuss the different maximum ^{1}H chemical shifts $\delta(^1H)_{max}$ of pyridine-acid complexes, 19 ppm in the solid state and 21 ppm in polar freon solution at low temperatures (Figure 12c). There is an

dx.doi.org/10.1021/jp305863n | J. Phys. Chem. A 2012, 116, 11370–11387

agreement[16,74−76] that in solution, at a given temperature, a distribution of different solvent configurations such as those depicted in Figure 16 is realized, where the exact distribution function and the size of the barrier in the configuration with the symmetric potential curve is difficult to elucidate.

In the solid state, as already discussed above, one might also conceive a rapidly fluctuating distribution of hydrogen bond geometries, arising from the excitation of intra- and intermolecular vibrations and phonons. Then, the larger maximum chemical shifts of the 1:1 acid−base complexes in solution as compared to the solid state might tentatively be explained with the presence of a larger amount of quasi-symmetric configurations in solution. However, further experimental and theoretical studies will be necessary to support this interpretation.

CONCLUSIONS

We arrive at the following conclusions of the present study.

(i) By enrichment of 4-methylpyridine (4-MP) with ^{15}N, multinuclear high-resolution ^{1}H, ^{2}H, and particularly ^{15}N solid state NMR allowed us to measure the chemical shifts of the hydrons and nitrogen atoms of the OHN hydrogen bridges formed between 4-MP and pentachlorophenol (PCP) in the solid state. By comparison with other pyridine-acid complexes, various hydrogen bond correlations have been improved which allow one to estimate OHN hydrogen bond geometries from NMR parameters. The observed H/D isotope effects on the hydron and nitrogen chemical shifts allow us then to estimate the corresponding isotope effects on the hydrogen bond geometries.

(ii) A complex isotopic phase diagram of 4-MPPCP was observed, where the main phases are triclinic 4-MPPCP-*h* exhibiting the strongest known OHN hydrogen bond and monoclinic 4-MPPCP-*d*, where D is located near oxygen. It could be shown that this isotopic polymorphism does not arise from isotope fractionation between the different forms—which is existent—but that it is the result of the geometric isotope effects observed. Deuteration increases the hydron−nitrogen distance and widens the hydrogen bridge, resulting in a reduction of the local dipole moment. This reduces the dipole−dipole interaction between different complexes (Figure 13) and other interactions take over, leading to a different crystal structure. It seems that H/D isotopic polymorphism is generally governed by geometric H/D isotope effects.

(iii) The influence of electric fields on the hydrogen bond geometry of 4-MPPCP is demonstrated by finding a displacement of the hydrogen bonded proton toward nitrogen, resulting in a zwitterionic structure. Nevertheless, a comparison of chemical shifts of pyridine-acid complexes in the solid state and in solution indicates that the proton in very strong OHN hydrogen bonds in polar liquid is more confined to the hydrogen bond center as compared to the solid state. The origin of this effect is related to a low-barrier hydrogen bond in the solid, whereas a distribution of no-barrier hydrogen bonds is postulated for the liquid, leading in this case to a solvent driven tautomerism.

Whereas the case of 4-MPPCP is spectacular, as replacement of a single H by D leads to isotopic polymorphism, this phenomenon does not seem to be uncommon in the case of fully deuterated organic molecules such as solid neat pyridine,[34] as mentioned in the Introduction. We think that also, in such a case, the polymorphism is caused by anharmonic zero-point vibrations which change slightly the carbon−hydrogen distances. This changes the van der Waals interactions between the molecules and eventually the crystal structure.

ASSOCIATED CONTENT

Supporting Information

Synthesis of 2-ethoxy-4-methyl-3,4-dihydro-2*H*-pyran (1). Synthesis of ^{15}N isotopic labeled 4-methylpyridine (2). Table S1: Relative deuterium fraction x_D of 4-MPPCP samples. Table S2: Temperature calibration *via* ^{15}N CPMAS NMR of 95% enriched TTAA (1,8-dihydro-5,7,12,14-tetramethyldibenzo-(b,i)-$^{15}N_4$-(1,4,8,11)-tetraazacyclotetra-deca-4,6,11,13-tetraene) at 60.6 MHz. Table S3: ^{15}N NMR chemical shift reference standards. Table S4: Acquisition parameters used to obtain the NMR spectra of pentachlorophenol-4-methylpyridine complexes in this work. Figures S1−S3: Liquid state ^{1}H NMR spectra (500 MHz) of pentachlorophenol in $CDCl_3$, of hexamethylbenzene (HMB), and of HMB-d_{18} in CD_2Cl_2, Solid state ^{1}H and ^{2}H MAS NMR spectra of HMB and of HMB-d_{18}, of an empty rotor. Figures S4−S6: ^{1}H MAS, ^{2}H, and ^{15}N MAS NMR spectra of 4-MPPCP at deuterium fractions of 0 and 0.35. Figure S7: (a) Correlation of ND - distances obtained for polycrystalline collidine-acid complexes by dipolar solid state NMR with the corresponding isotropic ^{15}N chemical shifts δ(OH<u>N</u>).[12] (b) Correlation between the $^{1}H-^{15}N$ scalar couplings J(O<u>H</u><u>N</u>) and the ^{15}N chemical shifts of pyridine-acid and collidine-acid complexes in CDF_3/CDF_2Cl at low temperatures. Adapted from ref 20b. Figure S8: Temperature dependent ^{15}N CPMAS spectra of the chemical shift thermometer TTAA.[43] This material is available free of charge via the Internet at http://pubs.acs.org.

AUTHOR INFORMATION

Corresponding Author

*E-mail: limbach@chemie.fu-berlin.de.

Present Addresses

[‖]University of Regensburg, Universitätsstr. 31, D-93040 Regensburg, Germany.

[⊥]Center for Magnetic Resonance, St. Petersburg State University, Universitetskiy prospect 26, 198504 Peterhof, Russia.

Notes

The authors declare no competing financial interest.

ACKNOWLEDGMENTS

We thank the reviewers of this manuscript for helpful comments, in particular concerning the origin of the isotopic polymorphism. This work has been supported by the Deutsche Forschungsgemeinschaft, the Fonds der Chemischen Industrie, Frankfurt, and the Russian Foundation of Basic Research (Project 11-03-00346).

REFERENCES

(1) Limbach, H. H.; Manz, J. *Bunsen-Ges. Phys. Chem., Ber.* **1998**, *102*, 289−291.

(2) (a) Cleland, W. W.; Kreevoy, M. M. *Science* **1994**, *264*, 1887−1890. (b) Frey, P. A.; Whitt, S. A.; Tobin, J. B. *Science* **1994**, *264*, 1927−1935. (c) Denisov, G. S.; Golubev, N. S.; Gindin, V. A.; Limbach, H. H.; Ligay, S. S.; Smirnov, S. N. *J. Mol. Struct.* **1994**, *322*, 83−91. (d) Shan, S.; Loh, S.; Herschlag, D. *Science* **1996**, *272*, 97−101. (e) Perrin, C. L. *Science* **1994**, *266*, 1665−1668. (f) Schowen, K. B.; Limbach, H. H.; Denisov, G. S.; Schowen, R. L. *Biochim. Biophys. Acta* **2000**, *1458*, 43−62.

(3) *Hydrogen Transfer Reactions*; Hynes, J. T., Klinman, J., Limbach, H. H., Schowen, R. L., Eds.; Wiley-VCH: Weinheim, Germany, 2007; Vols. *1*−*4*.
(4) (a) Gutberlet, T.; Heinemann, U.; Steiner, M. *Acta Crystallogr.* **2001**, *D57*, 349−354. (b) Blakeley, M. P.; Ruiz, F.; Cachau, R.; Hazemann, I.; Meilleur, F.; Mitschler, A.; Ginell, S.; Afonine, P.; Ventura, O. N.; Cousido-Siah, A.; et al. *Proc. Natl. Acad. Sci. U.S.A.* **2008**, *105*, 1844−1848.
(5) (a) Cooper, J. B.; Myles, D. A. A. *Acta Crystallogr.* **2000**, *D56*, 246−248. (b) Habash, J.; Raftery, J.; Nuttall, R.; Price, H. J.; Wilkinson, C.; Kalb, A. J.; Helliwell, J. R. *Acta Crystallogr.* **2000**, *D56*, 541−550. (c) Habash, J.; Raftery, J.; Weisgerber, S.; Cassetta, A.; Lehmann, M. S.; Hoghoj, P.; Wilkinson, C.; Campbell, J. W.; Helliwell, J. R. *J. Chem. Soc., Faraday Trans.* **1997**, *93*, 4313−4317.
(6) Fisher, S. Z.; Kovalevsky, A. Y.; Domsic, J. F.; Mustyakimov, M.; McKenna, R.; Silverman, D. N.; Langan, P. A. *Biochemistry* **2010**, *49*, 415−421.
(7) Brown, S. P.; Schnell, I.; Brand, J. D.; Müllen, K.; Spiess, H. W. *Phys. Chem. Chem. Phys.* **2000**, *2*, 1735−1745.
(8) Brunklaus, G.; Schauff, S.; Markova, D.; Klapper, M.; Müllen, K.; Spiess, H. W. *J. Phys. Chem. B* **2009**, *113*, 6674−6681.
(9) Akbey, Ü.; Granados-Focil, S.; Coughlin, E. B.; Graf, R.; Spiess, H. W. *J. Phys. Chem. B* **2009**, *113*, 9151−9160.
(10) Brown, S. P.; Zhu, X. X.; Saalwächter, K.; Spiess, H. W. *J. Am. Chem. Soc.* **2001**, *123*, 4275−4285.
(11) Benedict, H.; Limbach, H. H.; Wehlan, M.; Fehlhammer, W. P.; Golubev, N. S.; Janoschek, R. *J. Am. Chem. Soc.* **1998**, *120*, 2939−2950.
(12) Lorente, P.; Shenderovich, I. G.; Golubev, N. S.; Denisov, G. S.; Buntkowsky, G.; Limbach, H. H. *Magn. Reson. Chem.* **2001**, *39*, S18−S29.
(13) (a) Paik, Y.; Yang, C.; Metaferia, B.; Tang, S.; Bane, S.; Ravindra, R.; Shanker, N.; Alcaraz, A. A.; Johnson, S. A.; Schaefer, J.; et al. *J. Am. Chem. Soc.* **2007**, *129*, 361−370. (b) Cegelski, L.; Schaefer, J. *J. Biol. Chem.* **2005**, *280*, 39238−39245. (c) Opella, S. J.; Marassi, F. M. *Chem. Rev.* **2004**, *104*, 3587−3606.
(14) Agarwal, V.; Linser, R.; Fink, U.; Faelber, K.; Reif, B. *J. Am. Chem. Soc.* **2010**, *132*, 3187−3195.
(15) (a) Webber, A. L.; Elena, B.; Griffin, J. M.; Yates, J. R.; Pham, T. N.; Mauri, F.; Pickard, C. J.; Gil, A. M.; Stein, R.; Lesage, A.; Emsley, L.; Brown, S. P. *Phys. Chem. Chem. Phys.* **2010**, *12*, 6970−6983. (b) Pickard, C. J.; Salager, E.; Pintacuda, G.; Elena, B.; Emsley, L. *J. Am. Chem. Soc.* **2007**, *129*, 8932−8933. (c) Brown, S. P.; Zhu, X. X.; Saalwächter, K.; Spiess, H. W. *J. Am. Chem. Soc.* **2001**, *123*, 4275−4285.
(16) (a) Limbach, H. H.; Denisov, G. S.; Golubev, N. S. In *Isotope Effects In Chemistry and Biology*; Kohen, A., Limbach, H. H., Eds.; Taylor & Francis: Boca Raton, FL, 2005; Chapter 7, pp 193−230. (b) Detering, C.; Tolstoy, P. M.; Golubev, N. S.; Denisov, G. S.; Limbach, H. H. *Dokl. Phys. Chem.* **2001**, *379*, 1−4.
(17) Sharif, S.; Fogle, E.; Toney, M. D.; Denisov, G. S.; Shenderovich, I. G.; Tolstoy, P. M.; Chan-Huot, M.; Buntkowsky, G.; Limbach, H. H. *J. Am. Chem. Soc.* **2007**, *129*, 9558−9559.
(18) (a) Golubev, N. S.; Smirnov, S. N.; Gindin, V. A.; Denisov, G. S.; Benedict, H.; Limbach, H. H. *J. Am. Chem. Soc.* **1994**, *116*, 12055−12056. (b) Smirnov, S. N.; Golubev, N. S.; Denisov, G. S.; Benedict, H.; Schah-Mohammedi, P.; Limbach, H. H. *J. Am. Chem. Soc.* **1996**, *118*, 4094−4101. (c) Golubev, N. S.; Smirnov, S. N.; Schah-Mohammedi, P.; Shenderovich, I. G.; Denisov, G. S.; Gindin, V. A.; Limbach, H. H. *Russ. J. Gen. Chem.* **1997**, *67*, 1082−1087. (d) Shenderovich, I. G.; Smirnov, S. N.; Denisov, G. S.; Gindin, V. A.; Golubev, N. S.; Dunger, A.; Reibke, R.; Kirpekar, S.; Malkina, O. L.; Limbach, H. H. *Bunsen-Ges. Phys. Chem., Ber.* **1998**, *102*, 422−428. (e) Benedict, H.; Shenderovich, I. G.; Malkina, O. L.; Malkin, V. G.; Denisov, G. S.; Golubev, N. S.; Limbach, H. H. *J. Am. Chem. Soc.* **2000**, *122*, 1979−1988. (f) Shenderovich, I. G.; Limbach, H. H.; Smirnov, S. N.; Tolstoy, P. M.; Denisov, G. S.; Golubev, N. S. *Phys. Chem. Chem. Phys.* **2002**, *4*, 5488−5497. (g) Smirnov, S. N.; Benedict, H.; Golubev, N. S.; Denisov, G. S.; Kreevoy, M. M.; Schowen, R. L.; Limbach, H. H. *Can. J. Chem.* **1999**, *77*, 943−949.
(19) (a) Tolstoy, P. M.; Smirnov, S. N.; Shenderovich, I. G.; Golubev, N. S.; Denisov, G. S.; Limbach, H. H. *J. Mol. Struct.* **2004**, *700*, 19−27. (b) Tolstoy, P. M.; Guo, J.; Koeppe, B.; Golubev, N. S.; Denisov, G. S.; Smirnov, S. N.; Limbach, H. H. *J. Phys. Chem. A* **2010**, *114*, 10775−10782.
(20) (a) Limbach, H. H.; Pietrzak, M.; Benedict, H.; Tolstoy, P. M.; Golubev, N. S.; Denisov, G. S. *J. Mol. Struct.* **2004**, *706*, 115−119. (b) Limbach, H. H.; Pietrzak, M.; Sharif, S.; Tolstoy, P. M.; Shenderovich, I. G.; Smirnov, S. N.; Golubev, N. S.; Denisov, G. S. *Chem.—Eur. J.* **2004**, *10*, 5195−5204.
(21) (a) Sharif, S.; Denisov, G. S.; Toney, M. D.; Limbach, H. H. *J. Am. Chem. Soc.* **2007**, *129*, 6313−6327. (b) Sharif, S.; Schagen, D.; Toney, M. D.; Limbach, H. H. *J. Am. Chem. Soc.* **2007**, *129*, 4440−4455. (c) Sharif, S.; Chan Huot, M.; Tolstoy, P. M.; Toney, M. D.; Limbach, H. H. *J. Phys. Chem. B* **2007**, *111*, 3869−3876. (d) Sharif, S.; Denisov, G. S.; Toney, M. D.; Limbach, H. H. *J. Am. Chem. Soc.* **2006**, *128*, 3375−3387.
(22) Steiner, T. *J. Phys. Chem. A* **1998**, *102*, 7041−7052.
(23) Grech, E.; Kalenik, J.; Sobczyk, L. *J. Chem. Soc., Faraday Trans.* **1979**, *75*, 1587−1592.
(24) Kalenik, J.; Majerz, I.; Malarski, Z.; Sobczyk, L. *Chem. Phys. Lett.* **1990**, *165*, 15−18.
(25) Malarski, Z.; Rospenk, M.; Sobczyk, L.; Grech, E. *J. Phys. Chem.* **1982**, *86*, 401−406.
(26) Malarski, Z.; Majerz, I.; Lis, T. *J. Mol. Struct.* **1987**, *158*, 369−377 (file RAKQOJ in the Cambridge Structural Database (CSD)).
(27) Malarski, Z.; Majerz, I.; Lis, T. *J. Mol. Struct.* **1996**, *380*, 249−256.
(28) Steiner, T.; Majerz, I.; Wilson, C. C. *Angew. Chem., Int. Ed.* **2001**, *40*, 2651−2654.
(29) Majerz, I.; Malarski, Z.; Lis, T. *J. Mol. Struct.* **1990**, *240*, 47−58 (file GADGUN01 in the Cambridge Structural Database (CSD)).
(30) Ubbelohde, A. R.; Woodward, I. *Nature* **1939**, *144*, 632−632.
(31) Schmidtmann, M.; Farrugia, L. J.; Middlemiss, D. S.; Gutmann, M. J.; McIntyre, G. J.; Wilson, C. C. *J. Phys. Chem. A* **2009**, *113*, 13985−13997.
(32) Ford, S. J.; Delamore, O. J.; Evans, J. S. O.; McIntyre, G. J.; Johnson, M. R.; Evans, I. R. *Chem.—Eur. J.* **2011**, *17*, 14942−14951.
(33) Hughes, C. E.; Harris, K. D. M. *J. Phys. Chem. A* **2008**, *112*, 6808−6810.
(34) Crawford, S.; Kirchner, M. T.; Bläser, D.; Boese, R.; David, W. I. F.; Dawson, A.; Gehrke, A.; Ibberson, R. M.; Marshall, W. G.; Parsons, S.; et al. *Angew. Chem., Int. Ed.* **2009**, *48*, 755−757.
(35) Vasylyeva, V.; Kedziorski, T.; Metzler-Nolte, N.; Schauerte, C.; Merz, K. *Cryst. Growth Des.* **2010**, *10*, 4224−4226.
(36) Funnell, N. P.; Dawson, A.; Francis, D.; Lennie, A. R.; Marshall, W. G.; Moggach, S. A.; Warren, J. E.; Parsons, S. *Cryst. Eng. Commun.* **2010**, *12*, 2573−2583.
(37) Zhou, J.; Kye, Y. S.; Harbison, G. S. *J. Am. Chem. Soc.* **2004**, *126*, 8392−8393.
(38) Muller, P. *Pure Appl. Chem.* **1994**, *66*, 1077−1184. "Isotopomers" are isomers having the same number of each isotopic atom but differing in their positions, e.g., CH_3OD and CH_2DOH. "Isotopologues" represent molecular entities which differ only in the number of isotopic substitutions, e.g., CH_4, CH_3D, etc.
(39) Zhou, J.; Kye, Y. S.; Kolesnikov, A. I.; Harbison, G. S. *Isot. Environ. Health Stud.* **2006**, *42*, 271−277.
(40) Longley, R. I., Jr.; Emerson, W. S. *J. Am. Chem. Soc.* **1950**, *72*, 3079−3081.
(41) Whaley, T. W.; Ott, D. G. *J. Labelled Compd.* **1974**, *10*, 283−286.
(42) Kendrick, R. D.; Friedrich, S.; Wehrle, B.; Limbach, H. H.; Yannoni, C. S. *J. Magn. Reson.* **1985**, *65*, 159−161.
(43) Wehrle, B.; Aguilar-Parrilla, F.; Limbach, H. H. *J. Magn. Reson.* **1990**, *87*, 584−591.
(44) Aguilar-Parrilla, F.; Wehrle, B.; Bräunling, H.; Limbach, H. H. *J. Magn. Reson.* **1990**, *87*, 592−597.
(45) Stride, J. A.; Adams, J. M.; Johnson, M. R. *Chem. Phys.* **2005**, *317*, 143−152.

(46) Solid NH_4Cl has been shown to resonate at −341.168 ppm with respect to external liquid nitromethane by: Hayashi, S.; Hayamizu, K. *Bull. Chem. Soc. Jpn.* **1991**, *64*, 688−690.
(47) Pauling, L. *J. Am. Chem. Soc.* **1947**, *69*, 542−553.
(48) Brown, I. D. *Acta Crystallogr.* **1992**, *B48*, 553−572.
(49) Gilli, P.; Bertolasi, V.; Ferretti, V.; Gilli, G. *J. Am. Chem. Soc.* **1994**, *116*, 909−915.
(50) Steiner, T. J.; Saenger, W. *Acta Crystallogr.* **1994**, *B50*, 348−357.
(51) Vener, M. V.; Manaev, A. V.; Egorova, A. N.; Tsirelson, V. G. *J. Phys. Chem. A* **2007**, *111*, 1155−1162.
(52) (a) Ubbelohde, A. R.; Gallagher, K. J. *Acta Crystallogr.* **1995**, *8*, 71−83. (b) Legon, A. C.; Millen, D. J. *Chem. Phys. Lett.* **1988**, *147*, 484−489. (c) Sokolov, N. D.; Savel'ev, V. A. *Chem. Phys.* **1977**, *22*, 383−399. (d) Sokolov, N. D.; Savel'ev, V. A. *Chem. Phys.* **1994**, *181*, 305−317.
(53) Limbach, H. H.; Tolstoy, P. M.; Pérez-Hernández, N.; Guo, J.; Shenderovich, I. G.; Denisov, G. S. *Isr. J. Chem.* **2009**, *49*, 199−216.
(54) (a) Ernst, M.; Bush, S.; Kolbert, A. C.; Pines, A. *J. Chem. Phys.* **1996**, *105*, 3387−3397. (b) Ernst, M.; Zimmermann, H.; Meier, B. H. *Chem. Phys. Lett.* **2000**, *317*, 581−588.
(55) Amornsakchai, P.; Hodgkinson, P.; Harris, R. K. *Mol. Phys.* **2004**, *102*, 877−882.
(56) Foces-Foces, C.; Llamas-Saiz, C. A. L.; Lorente, P.; Golubev, N. S.; Limbach, H. H. *Acta Crystallogr.* **1999**, *C55*, 377−381.
(57) Heilbronner, E.; Günthard, H. H.; Gerdil, H. R. *Helv. Chim. Acta* **1956**, *39*, 1171−1181.
(58) Shibl, M. F.; Pietrzak, M.; Limbach, H. H.; Kühn, O. *ChemPhysChem* **2007**, *8*, 315−321.
(59) Schah-Mohammedi, P.; Shenderovich, I. G.; Detering, C.; Limbach, H. H.; Tolstoy, P. M.; Smirnov, S. N.; Denisov, G. S.; Golubev, N. S. *J. Am. Chem. Soc.* **2000**, *122*, 12878−12879.
(60) Ramos, M.; Alkorta, I.; Elguero, J.; Golubev, N. S.; Denisov, G. S.; Benedict, H.; Limbach, H. H. *J. Phys. Chem. A* **1997**, *101*, 9791−9800.
(61) Janoschek, R.; Weidemann, E. G.; Pfeiffer, H.; Zundel, G. *J. Am. Chem. Soc.* **1972**, *94*, 2387−2396.
(62) (a) Shenderovich, I. G.; Tolstoy, P. M.; Golubev, N. S.; Smirnov, S. N.; Denisov, G. S.; Limbach, H. H. *J. Am. Chem. Soc.* **2003**, *125*, 11710−11720. (b) Shenderovich, I. G.; Limbach, H. H.; Smirnov, S. N.; Tolstoy, P. M.; Denisov, G. S.; Golubev, N. S. *Phys. Chem. Chem. Phys.* **2002**, *4*, 5488−5497.
(63) Tolstoy, P. M.; Schah-Mohammedi, P.; Smirnov, S. N.; Golubev, N. S.; Denisov, G. S.; Limbach, H. H. *J. Am. Chem. Soc.* **2004**, *126*, 5621−5634.
(64) Emmler, T.; Gieschler, S.; Limbach, H. H.; Buntkowsky, G. *J. Mol. Struct.* **2004**, *700*, 29−38.
(65) Shenderovich, I. G.; Buntkowsky, G.; Schreiber, A.; Gedat, E.; Sharif, S.; Albrecht, J.; Golubev, N. S.; Findenegg, G. H.; Limbach, H. H. *J. Phys. Chem. B* **2003**, *107*, 11924−11939.
(66) Khan, M.; Enkelmann, V.; Brunklaus, G. *J. Am. Chem. Soc.* **2010**, *132*, 5254−5263.
(67) Kong, S.; Borissova, A. O.; Lesnichin, S. B.; Hartl, M.; Daemen, L. L.; Eckert, J.; Antipin, M. Y.; Shenderovich, I. G. *J. Phys. Chem. A* **2011**, *115*, 8041−8048.
(68) Perrin, C. L.; Karri, P. *Chem. Commun.* **2010**, *46*, 481−483.
(69) (a) Bigeleisen, J.; Mayer, M. G. *J. Chem. Phys.* **1947**, *15*, 261−267. (b) Bigeleisen, J. In *Isotope Effects In Chemistry and Biology*; Kohen, A., Limbach, H. H., Eds.; Taylor & Francis: Boca Raton, FL, 2005; Chapter 1, pp 1−40.
(70) (a) Pietrzak, M.; Shibl, M. F.; Bröring, M.; Kühn, O.; Limbach, H. H. *J. Am. Chem. Soc.* **2007**, *129*, 296−304. (b) Lopez del Amo, J. M.; Langer, U.; Torres, V.; Pietrzak, M.; Buntkowsky, G.; Vieth, H. M.; Shibl, M. F.; Kühn, O.; Broering, M.; Limbach, H. H. *J. Phys. Chem. A* **2009**, *113*, 2193−2206.
(71) Muller, N.; Reiter, R. C. *J. Chem. Phys.* **1965**, *42*, 3265−3269.
(72) Dumez, J. N.; Pickard, C. J. *J. Chem. Phys.* **2009**, *130*, 104701.
(73) (a) Golubev, N. S.; Denisov, G. S.; Smirnov, S. N.; Shchepkin, D. N.; Limbach, H. H. *Z. Phys. Chem.* **1996**, *196*, 73−84. (b) Guo, J.; Koeppe, B.; Tolstoy, P. M. *Phys. Chem. Chem. Phys.* **2011**, *13*, 2335−2341.
(74) Shenderovich, I. G.; Burtsev, A. P.; Denisov, G. S.; Golubev, N. S.; Limbach, H. H. *Magn. Reson. Chem.* **2001**, *39*, S91−S99.
(75) Koeppe, B.; Tolstoy, P. M.; Limbach, H. H. *J. Am. Chem. Soc.* **2011**, *133*, 7897−7908.
(76) (a) Perrin, C. L.; Ohta, B. K. *J. Mol. Struct.* **2001**, *644*, 1−12. (b) Perrin, C. L.; Lau, J. S. *J. Am. Chem. Soc.* **2006**, *128*, 11820−11824. (c) Perrin, C. L.; Lau, J. S.; Ohta, B. K. *Pol. J. Chem.* **2003**, *77*, 1693−170. (d) Perrin, C. L. *Acc. Chem. Res.* **2010**, *43*, 1550−1557.